

A Comprehensive *GALEX* Ultraviolet Catalog of Star Clusters in M31 and a Study of the Young Clusters

Yongbeom Kang^{1,2}, Soo-Chang Rey^{1,4}, Luciana Bianchi², Kyungsook Lee¹, YoungKwang Kim¹, and Sangmo Tony Sohn³

ybkang@cnu.ac.kr, screy@cnu.ac.kr

Received _____; accepted _____

revised Dec, 08, 2011

¹Department of Astronomy and Space Science, Chungnam National University, Daejeon 305-764, Korea

²Department of Physics and Astronomy, Johns Hopkins University, Baltimore, MD 21218, USA

³Space Telescope Science Institute, Baltimore, MD 21218, USA

⁴Author to whom any correspondence should be addressed

ABSTRACT

We present a comprehensive catalog of 700 confirmed star clusters in the field of M31 compiled from three major existing catalogs. We detect 418 and 257 star clusters in *Galaxy Evolution Explorer* (*GALEX*) near-ultraviolet (NUV) and far-ultraviolet (FUV) imaging, respectively. Our final catalog includes photometry of star clusters in up to 16 passbands ranging from FUV to NIR as well as ancillary information such as reddening, metallicity, and radial velocities. In particular, this is the most extensive and updated catalog of UV integrated photometry for M31 star clusters. Ages and masses of star clusters are derived by fitting the multi-band photometry with model spectral energy distribution (SED); UV photometry enables more accurate age estimation of young clusters. Our catalog includes 182 young clusters with ages less than 1 Gyr. Our estimated ages and masses of young clusters are in good agreement with previously determined values in the literature. The mean age and mass of young clusters are about 300 Myr and $10^4 M_{\odot}$, respectively. We found that the compiled $[\text{Fe}/\text{H}]$ values of young clusters included in our catalog are systematically lower (by more than 1 dex) than those from recent high-quality spectroscopic data and our SED fitting result. We confirm that most of the young clusters kinematics show systematic rotation around the minor axis and association with the thin disk of M31. The young clusters distribution exhibits a distinct peak in the M31 disk around 10 - 12 kpc from the center and follow a spatial distributions similar to other tracers of disk structure such as OB stars, UV star-forming regions, and dust. Some young clusters also show concentration around the ring splitting regions found in the southern part of the M31 disk and most of them have systematically younger (< 100 Myr) ages. Considering the kinematical properties and spatial distribution of young clusters, they might be associated with the well-known 10 kpc star-

formation ring structure in the M31 disk. Consequently, we suggest that various properties of young clusters in M31 might be in line with the scenarios that a satellite galaxy had passed through the disk of M31 less than few hundred million years ago.

Subject headings: galaxies: evolution — galaxies: individual(M31) — galaxies: star clusters — galaxies: structures — ultraviolet: galaxies

1. Introduction

In the galaxy formation scenario based on the cold dark matter models, galaxies build up hierarchically (White & Rees 1978; White & Frenk 1991; Springel et al. 2005). In this scenario, merging and accretion play key roles over cosmic time. From high redshift to the nearby universe, many massive galaxies show evidence of ongoing merging and/or accretion. In this context, large disk galaxies like the Milky Way (MW) and M31 are also thought to have assembled a significant fraction of their mass through interactions with other small galaxies (e.g., Ibata et al. 2001). Most of these interactions change the morphology and star formation history of the galaxy.

As a typical spiral galaxy in the nearby Universe (Hammer et al. 2007), M31 provides a unique and most important opportunity for testing this scenario on external spiral galaxies due to its proximity (785 kpc; McConnachie et al. 2005). Many recent studies have suggested that M31 is a promising example, exhibiting a hint of a past merger (Block et al. 2006; Brown et al. 2006; Gordon et al. 2006; Ibata et al. 2007; Mori & Rich 2008; McConnachie et al. 2009). Most observational and theoretical results concern the halo and outer disk of M31. Especially, previous photometric and spectroscopic observations suggest that merging events have played an important role in the construction and evolution of the halo of M31 (McConnachie et al. 2009 and references therein).

Recently, in addition to the well-known 10 kpc ring seen in previous observations (Gordon et al. 2006 and references therein), the presence of a second, inner dust ring was discovered in the disk of M31 (Block et al. 2006). While a detailed study of the origin of the ring structure of M31 is needed, the two off-center circular rings suggest that the disk of M31 has been distorted by a very recent passage of its satellite galaxy through the disk (i.e., a head-on collision with the satellite galaxy about a few tens or hundreds Myr ago, Gordon et al. 2006; Block et al. 2006). In this case, such a recent event may have enhanced

the efficiency of star formation in the disk of M31 (e.g., Yin et al. 2009).

Star cluster systems can be a tracer of galaxy formation and assembly, in the sense that significant star cluster formation is typically produced by major star-forming episodes in a galaxy (Larsen & Richtler 2000; Brodie & Strader 2006). More than 400 globular clusters (GCs) are known in M31 (e.g., Peacock et al. 2010), which is about a factor of three more than in the MW. The GC system of M31 has two subpopulations, one is a metal-rich and spatially concentrated subpopulation and the other is metal-poor and spatially extended. The metal-rich GCs show “bulge-like” kinematics with rotation (Perrett et al. 2002; Lee et al. 2008). However, unlike in the MW, the metal-poor GCs also show significant rotation (Huchra et al. 1991; Perrett et al. 2002; Lee et al. 2008). Morrison et al. (2004) showed a thin disk population of GCs which constitutes about 27 % of the Perrett et al. (2002) sample. Subsequently, it has been shown that at least a subset of these objects are in fact young (≤ 1 Gyr), metal-rich star clusters rather than old metal-poor GCs (Beasley et al. 2004; Burstein et al. 2004; Fusi Pecci et al. 2005; Puzia et al. 2005; Rey et al. 2007; Caldwell et al. 2009; Perina et al. 2010).

In contrast to the MW, a large population of young clusters with ages less than 1 - 2 Gyr is found in M31 (Burstein et al. 2004; Beasley et al. 2004, 2005; Fusi Pecci et al. 2005; Puzia et al. 2005; Rey et al. 2007; Caldwell et al. 2009; Peacock et al. 2010). Fusi Pecci et al. (2005) presented 67 young clusters from the Revised Bologna Catalog (RBC, Galleti et al. 2004) showing blue optical colors $[(B - V)_0 < 0.45]$ and/or high strength of $H\beta$ spectral index ($H\beta > 3.5 \text{ \AA}$). Rey et al. (2007) confirmed these young clusters using *Galaxy Evolution Explorer* (*GALEX*) ultraviolet (UV) photometry and suggested that the existence of young clusters in the outskirts of the M31 disk is due to the occurrence of significant recent star formation in the thin-disk. More recently, two comprehensive catalogs of young clusters in M31 have been published from the

spectroscopic survey of Caldwell et al. (2009) and the Sloan Digital Sky Survey (SDSS) data of Peacock et al. (2010). Caldwell et al. (2009) estimated ages and masses of 140 young clusters and Peacock et al. (2010) defined 156 young clusters with blue colors of $g - r < 0.3$. Most of these clusters are more massive (between 10^3 and $10^5 M_\odot$) than the Galactic open clusters (Caldwell et al. 2009). Furthermore, they have similar characteristics to the blue star clusters in the LMC (Burstein et al. 2004; Fusi Pecci et al. 2005) and other massive young clusters in Local Group galaxies (Barmby et al. 2009). However, no such predominant counterparts have yet been discovered in the disk of the MW, except for a handful of massive young clusters identified in the center of the MW (e.g., Messineo et al. 2009). The existence of massive young clusters in the outskirts of the M31 disk indicates the occurrence of significant recent star formation in the disk of M31 (Fusi Pecci et al. 2005; Rey et al. 2007; Caldwell et al. 2009). Assuming that merging and accretion event triggered higher-level star formation in the disk of M31 than in quiescent galactic disks, it is interesting to examine the properties of star clusters related to the M31 disk, elucidating the recent star formation history in M31.

Motivated by the opportunity to study formation and evolution of young clusters in M31, in this paper we construct a comprehensive multi-band catalog of star clusters in M31 compiled from RBC, Caldwell et al. (2009, 2011), and Peacock et al. (2010) samples. In particular, we included *GALEX* UV data, since the UV flux is highly sensitive to young main-sequence stars included in the massive young clusters which radiate more UV flux than in optical passbands (Rey et al. 2007; Kaviraj et al. 2007). We select extensive subsamples of young clusters which is complementary with previous catalogs of young clusters in M31 (e.g., Caldwell et al. 2009). Various properties (age, mass, metallicity, kinematics, and spatial distribution) of young clusters are compared with star-forming (SF) regions and OB type stars in M31, and with the 10 kpc ring structure. This allows us to test whether most young clusters may be the possible outgrowth of a recent accretion of

satellite galaxy occurred at the center of the M31 disk.

In Section 2, we describe optical and near-infrared (NIR) data of the M31 star clusters compiled from previous catalogs. Combining additional *GALEX* UV data and other auxiliary information, we present a final merged catalog of star clusters in M31. In Section 3, by comparing observed spectral energy distributions (SEDs) with simple stellar population models, we estimate ages and masses of star clusters and select young clusters. We present properties of young clusters in Section 4. We also discuss the relationship between young clusters and M31 disk structures in terms of possible recent star formation history in the M31 disk. The conclusions are summarized in Section 5.

2. Data

2.1. Photometric Data

2.1.1. Optical and Near-infrared Data

Large catalogs of star clusters in M31 have been published in the past decade (e.g., Barmby et al. 2000; Galleti et al. 2004; Kim et al. 2007; Caldwell et al. 2009, 2011; Peacock et al. 2010). However, it is still a challenge to build a complete, deep, and homogeneous catalog of star clusters in M31. For example, it is not easy to detect relatively faint star clusters which are mainly projected onto the bright disk structure or bulge of M31. Furthermore, some of the star clusters exist in the halo, far away from the host galaxy (Huxor et al. 2008), requiring wide-field surveys of the outer halo of M31.

One of the most self-consistent catalogs of star clusters in M31 is that of Barmby et al. (2000), in which they presented *UBVRI* and *JHK* photometry of 435 clusters and cluster candidates. However, only for 268 objects optical photometry in four or more

bands is available, and 224 have NIR photometry. Galleti et al. (2004) identified 693 clusters and cluster candidates from the 2 Micron All Sky Survey (2MASS) database. They provide an extensive RBC which includes compiled multi-band optical data from many previous catalogs. Kim et al. (2007) carried out wide field observations and found 113 new genuine star clusters and 258 probable star clusters which are mostly faint ($18 \leq V \leq 20$ mag) objects. Caldwell et al. (2009) published a new catalog of 670 likely star clusters, with accurate coordinates from the Local Group Galaxy Survey (LGGS, Massey et al. 2006) and the Digitized Sky Survey (DSS) data. Most of these clusters are confirmed based on high-quality spectra taken with the Hectospec spectrograph on the 6.5 m MMT. These authors also estimated ages, reddening values, and masses of 140 young clusters by comparing the observed spectra with model ones. They presented only V -band photometry for 510 clusters from the LGGS images, with no information on colors. Based on the classification of Caldwell et al. (2009), subsequently Caldwell et al. (2011) also provided metallicities and ages of 367 old clusters using the high-quality spectra. Peacock et al. (2010) presented an updated catalog including new, consistent $ugriz$ and K -band photometry based on images from the SDSS and Wide Field CAMera (WFCAM) on the UK Infrared Telescope (UKIRT). This catalog includes homogeneous photometry of 572 clusters and 373 candidate clusters. Using archival images from the LGGS, Fan et al. (2010) recently presented an updated $UBVRI$ photometric catalog containing 970 objects selected from the RBC.

For our following analysis, we construct a new compiled catalog of star clusters in M31 carefully considering three previously published catalogs: RBC version 4 (v4), Caldwell et al. (2009, 2011), and Peacock et al. (2010). Our catalog is mainly based on the RBC v4 which is the most extensive and commonly used catalog although it contains rather heterogeneous photometry compiled from various literature (Galleti et al. 2004). As of December 2009, the RBC v4 includes most previous data, except for the catalogs

of Peacock et al. (2010) and Caldwell et al. (2011), and contains 667 star clusters and 606 candidate clusters. We carefully compared names and coordinates of star clusters between the RBC v4, Caldwell et al. (2009, 2011), and Peacock et al. (2010) catalogs. While most objects are well matched in these catalogs, some have slightly different coordinates in the RBC v4. From inspection of LGGS and SDSS images, we found the coordinates of 17 objects provided by RBC v4 to be discrepant with real centers of the objects and finalized their coordinates with those of Caldwell et al. (2009, 2011). These are B284, B353, B414, NB18, NB42, NB44, NB104, B001D, B003D, B246D, B306D, DAO89, V203, M075, M088, BH01, BH07. We add 56 objects from the catalogs of Caldwell et al. (2009, 2011) and Peacock et al. (2010) which are not contained in the RBC v4. These are previously known objects however they are not included in the RBC v4.

The final compiled catalog contains a total of 2,101 objects. This catalog contains star clusters, candidate clusters, HII regions, stars, asterisms, and background galaxies classified from RBC v4, Caldwell et al. (2009, 2011), and Peacock et al. (2010). Some objects do not have the same classification in these three catalogs. In this paper, we only consider 700 star clusters which are classified as confirmed star clusters at least in one of three catalogs. As a result our compiled catalog is the most extensive one for confirmed star clusters in M31 (see Section 2.3 and Table 1).

2.1.2. *GALEX Ultraviolet Data*

UV data is very powerful tool for breaking age-metallicity degeneracy and estimating the ages of star clusters (Kaviraj et al. 2007; Bianchi 2009, 2011). We used UV images from the Nearby Galaxy Survey (NGS) obtained by *GALEX* in two UV bands: far-ultraviolet (FUV; 1350 - 1750 Å) and near-ultraviolet (NUV; 1750 - 2750 Å). Every *GALEX* image has 1.25 deg circular field of view (Morrissey et al. 2007). A total of 23 images (about 17

square degrees) have covered most of the disk and halo of M31. The details of the *GALEX* observations for M31 are presented in Rey et al. (2005, 2007).

Of each image, we only use the inner 1.1 deg field to avoid the distortion at the edge of the field. Aperture photometry of all point sources in the M31 fields was carried out using the DAOPHOTII package (Stetson 1987). We measured the flux of each source within 3 pixel (4.5 arcsec) radius and applied aperture correction using isolated stars in each image. The measured fluxes were converted to the AB magnitude system with the calibration of Morrissey et al. (2007). Our UV photometry is the same as that published by Rey et al. (2007). Sources in our *GALEX* photometry were cross-matched with clusters in our compiled catalog using a matching radius of 6 arcsec. We then carried out careful visual inspection of all matched objects in each *GALEX* image and reject all spurious sources (i.e., sources highly contaminated by nearby objects, faint fuzzy sources, and noisy pixels). Out of the 700 star clusters in the compiled catalog, 418 ($\sim 60\%$) and 257 ($\sim 37\%$) objects are detected in the *GALEX* NUV and FUV band, respectively. Of these, 302 and 167 objects were detected in the previous NUV and FUV data of Rey et al. (2007). The limiting magnitudes of star clusters are 23.6 mag and 23.7 mag for FUV and NUV, respectively.

In Figure 1, we present the spatial distribution of the star clusters detected in *GALEX* NUV and FUV bands with respect to the M31 disk, NGC 205, and M32. We examine the detection rate of star clusters in our *GALEX* fields with respect to their B and V magnitudes. Figure 2 shows the fraction of star clusters detected in the NUV and FUV bands as a function of V magnitude and $B - V$ color. Of the 484 clusters with both B and V data, 328 (about 68 %) and 191 (about 39 %) clusters are detected in the *GALEX* NUV and FUV, respectively. The color-magnitude diagrams and color histogram show that most of the detected objects are optically blue clusters with $B - V < 1.2$. Many of the bluest clusters with $B - V < 0.5$ are detected in the *GALEX* UV bands even though they

are fainter ($V > 16$) than the redder clusters in the optical passband. Most of these blue clusters are young clusters (see Section 3).

2.2. Auxiliary Data: Reddening, Metallicity, and Radial Velocity

We used reddening values of star clusters from Barmby et al. (2000), Fan et al. (2008), and Caldwell et al. (2009, 2011). Barmby et al. (2000) and Fan et al. (2008) estimated the reddening values from reddening-free parameters and color-metallicity relation. Caldwell et al. (2009, 2011) published reddening values of young and old clusters, separately, which were derived by comparing the observed spectra with model ones. The mean differences between reddening values of Caldwell et al. (2009, 2011) and those of Barmby et al. (2000) and Fan et al. (2008) are +0.03 for both cases. In the case of star clusters with available reddening values in more than two different works, the average value has been adopted. The reddening values are available for 555 star clusters in our compiled catalog.

As for the 145 star clusters with no available reddening values in the literature, using 555 star clusters with available reddening values, we calculate median reddening values of star clusters located within an annulus at every 2 kpc radius from the center of M31. Figure 3 shows the distribution of our compiled reddening values of 555 star clusters and calculated median reddening values of each annulus. As we can expect, the reddening values are maximum around the 10 kpc star formation ring in the M31 disk. Finally, we adopt the median reddening value of each annulus for star clusters with no available reddening estimates. However, beyond a galactocentric distance of 22 kpc, the reddening values converge to $E(B - V) = 0.13$ mag which is similar to the mode value of all old GCs of Caldwell et al. (2011). We adopt the $E(B - V) = 0.13$ mag for the star clusters at distances larger than 22 kpc, since most of them are located in halo regions.

From their Hectospec spectroscopic observations, Caldwell et al. (2011) presented metallicity values of 333 old clusters. Currently, this is the most extensive and homogeneous metallicity data-set. We adopt their metallicity values as a basic data, and also combine other metallicity values from Galleti et al. (2009), Perrett et al. (2002), and Barmby et al. (2000). The mean differences between metallicity values of Caldwell et al. (2011) and others are -0.07 for Galleti et al. (2009), $+0.05$ for Perrett et al. (2002), and $+0.14$ for Barmby et al. (2000). Finally, we adopt the mean value of metallicity from these works. For star clusters with metallicity value in only one paper, we adopt that value. The metallicity values are available for 399 star clusters in our compiled catalog.

The RBC v4 includes radial velocities of 528 star clusters as weighted mean values from various literature (e.g., Barmby et al. 2000; Perrett et al. 2002; Galleti et al. 2006; Kim et al. 2007; Caldwell et al. 2009; Alves-Brito et al. 2009). However, RBC v4 was not updated with the most recent data by Caldwell et al. (2011) for 507 star clusters. The mean difference between radial velocities of the RBC v4 and Caldwell et al. (2011) is about 3 km s^{-1} . Finally, we adopt the mean value of radial velocity from these two catalogs when more than one measurement is available. The final radial velocities are available for 617 star clusters in our compiled catalog.

2.3. Merged Catalog of Star Clusters in M31

Our final merged catalog of M31 star clusters is presented in Table 1. This catalog includes 700 star clusters with photometry in up to 16 passbands ranging from FUV to NIR as well as ancillary information such as reddening values, metallicity values, and radial velocities. Optical U, B, V, R, I and NIR J, H, K bands are from the RBC v4. Optical u, g, r, i, z and NIR K bands are from Peacock et al. (2010). Our compiled catalog is then used for the selection and analysis of young clusters in the following Sections. This is the

most extensive and updated catalog of UV photometry for M31 star clusters, superseding our previous UV catalog (Rey et al. 2007). The following is a brief description of each column of Table 1;

- *Column* (1): name of star cluster
- *Column* (2) - (3): coordinates of star cluster (hh:mm:ss, dd:mm:ss)
- *Column* (4): *GALEX* FUV magnitude (AB mag)
- *Column* (5): uncertainty of FUV magnitude (AB mag)
- *Column* (6): *GALEX* NUV magnitude (AB mag)
- *Column* (7): uncertainty of NUV magnitude (AB mag)
- *Column* (8) - (15): *U, B, V, R, I, J, H, K* magnitudes from RBC v4 (VEGA mag)
- *Column* (16) - (20): *u, g, r, i, z* magnitudes from Peacock et al. (2010) (AB mag)
- *Column* (21): *K* magnitude from Peacock et al. (2010) (VEGA mag)
- *Column* (22): reddening value
- *Column* (23): uncertainty of reddening value, obtained from compilation of different sources
- *Column* (24): [Fe/H] value
- *Column* (25): uncertainty of [Fe/H] value
- *Column* (26): radial velocity (km s⁻¹)
- *Column* (27): uncertainty of radial velocity (km s⁻¹)

- *Column* (28): classification flag of RBC v4 (1: cluster, 2: candidate cluster, 3: controversial object, 4: galaxy, 5: HII region, 6: star, 7: asterism, 8: extended cluster, 99: no data)
- *Column* (29): classification flag of Peacock et al. (2010) (1: old cluster, 2: candidate cluster, 3: young cluster, 4: galaxy, 5: HII region, 6: star, 99: no data)
- *Column* (30): classification flag of Caldwell et al. (2009, 2011) (1: young cluster (age < 1 Gyr), 2: intermediate cluster ($1 < \text{age} < 2$ Gyr), 3: old cluster (age > 2 Gyr), 4: cluster (no age), 5: star, 6: maybe star, 7: HII region, 8: unknown, 9: candidate cluster, 10: weird (SNR, Eta Carina type, or symbiotic star), 99: no data)
- *Column* (31): flag of $E(B - V)$ (1: mean value of reddening from available literature, 2: median reddening value of star clusters located within an annulus at every 2 kpc radius from the center of M31, 3: foreground reddening value of $E(B - V) = 0.13$ mag)

3. Selection of Young Clusters

3.1. Multi-band SED Fitting of Star Clusters

In order to estimate accurate ages and masses of the star clusters using multi-band SED fitting, we need many photometric data points covering as wide a wavelength range as possible (de Grijs et al. 2003; Anders et al. 2004; Kaviraj et al. 2007; Wang et al. 2010; Fan et al. 2010). In particular, UV photometry with optical one produces age constraints comparable to those of spectroscopic observations (Kaviraj et al. 2007). Our compiled catalog includes extensive photometric data in 16 bands from FUV to NIR. On the other hand, the photometric uncertainties are also important. Since the $UBVRI$ data are from RBC v4, we adopt photometric uncertainties following Galleti et al. (2004), i.e., ± 0.05 mag in $BVRI$ and ± 0.08 mag in U . We also adopt a typical error (± 0.05 mag) for the JHK

data from RBC v4. Peacock et al. (2010) present *ugriz* and *K* data and their photometric uncertainties. However, most of these uncertainties are extremely small, therefore we added a 0.05 mag uncertainty in all bands to account for zero-point inconsistencies among the various datasets. The photometric uncertainties of our *GALEX* FUV and NUV data are included in Table 1.

Basically, the multi-band SED fitting method is a comparison between multi-band photometry and synthetic model magnitudes of simple stellar population (SSP). A SSP is defined as a single generation of coeval stars characterized by fixed parameters such as metallicity, age, and stellar initial mass function (IMF). Synthetic SSP models are calculated on the basis of a set of evolutionary tracks of stars of different initial masses, combined with stellar spectra at different evolutionary stages. In this paper, we compare the multi-band SEDs of our star clusters with magnitudes constructed from progressively reddened PADUA SSP models (see Bianchi 2011) to estimate their ages. We use a Salpeter (1955) IMF with lower and upper mass limits of $0.10 M_{\odot}$ and $100 M_{\odot}$. After age and extinction are constrained from the SED colors, scaling the best-fit model to the observed magnitudes yields the cluster mass, since the distance is known.

Since the reddening is critical for an accurate age estimation of star clusters, we explored two ways for adopting a final reddening value. First, we adopted the reddening value from our merged catalog (“*indivEBV*”) and only derived the cluster age from SED fitting, imposing the adopted $E(B - V)$. The second way was to treat both age and $E(B - V)$ as free parameters in the SED fitting analysis (“*freeEBV*”). The *freeEBV* is important for the 145 star clusters whose reddening values are not available in the literature (see Section 2.2). Since the UV extinction curve of M31 is similar to that of MW (Bianchi et al. 1996), we assumed MW-type interstellar reddening ($R_V = 3.1$) (see Kang et al. 2009 for a discussion of the effects of different extinction curves). For our

SED fitting analysis, we used model grids with five different metallicities, $Z = 0.0004$, 0.004, 0.008, 0.02 (solar metallicity), and 0.05, although M31 is believed to have a higher metallicity than the MW (e.g., Massey 2003 and references therein). In this paper, we did not consider metallicities lower than $Z = 0.0004$, since we focus on the young clusters which are mostly metal-rich with $[\text{Fe}/\text{H}] > -1.0$ (see Section 4.2). We ran the SED fittings using each metallicity for all star clusters, in order to assess the effects of this parameter.

We compared the *freeEBV* results from SED-fitting with the literature values of $E(B - V)$ (*indivEBV*). There is good agreement for part of the sample (28 % of the whole final sample have $E(B - V)$ in agreement within $\Delta E(B - V) = 0.1$ mag) while other sources have larger discrepancies. The *freeEBV* values tend to be lower than literature values, but the mean difference is not significant (mean $\Delta E(B - V) \sim 0.09$ mag with a σ of 0.19 mag). The adopted extinction curve, and model details, may also affect the results. More important for our purpose is the effect of the uncertainty in $E(B - V)$ on the derived ages. We must recall first of all that for some of the catalog magnitudes compiled and used here, no errors are reported, which prevents derivation of formal errors from the SED fitting procedure (a constant uncertainty of some reasonable value has to be assumed for the *UBVR IJHK* photometry). Therefore, we estimated the robustness of the SED-based results by comparison with $E(B - V)$ from previous works. Figure 6 shows how the $E(B - V)$ uncertainty affects the derived ages. Where there is agreement in the derived $E(B - V)$ (e.g., within 0.1 mag, for 37 % of the clusters if we used the results from *FNugriz* assuming $Z=0.02$), obviously ages are in good agreement. In some cases where high discrepancies are seen, these may be due to some mismatch in SEDs between instruments (for example due to nearby objects), or to several minima being possible in the SED fitting. Overall, we see that the extraction of the "young clusters" subsample is not affected by these uncertainties.

In our SED fitting, we separated *UBVRI* data from *ugriz* data in order to keep the homogeneity of optical data. We also separated *JHK* (RBC v4) from *K* (Peacock et al. 2010) data. We considered four combinations of photometric passbands for our SED fitting. We include our UV data in each case. They are: (1) FUV, NUV, and *ugriz* (“F*Nugriz*”), (2) FUV, NUV, and *UBVRI* (“F*NUBVRI*”), (3) FUV, NUV, *ugriz*, and *K* (“F*NugrizK*”), and (4) FUV, NUV, *UBVRI*, and *JHK* (“F*NUBVRIJHK*”). In Figure 4, we present a sample (B100) of SED fitting results with four different band combinations. The estimated ages are similar between four different results. However, in many cases of F*NUBVRIJHK*, the photometry in *JHK* bands shows obvious offsets from UV and optical bands, probably due to the low resolution of 2MASS (see Figure 5). *GALEX* resolution is also low ($\sim 5''$), UV-bright objects are rare, compared with IR sources, and contamination is less likely, although possible. The F*NugrizK* provides a homogeneous dataset, therefore we did not consider the F*NUBVRIJHK* in our final SED fitting analysis. SED analysis requires photometric measurements in at least three passbands. We run the SED fitting for combinations of five different metallicities, two different reddening treatments, and three photometric combinations of different passbands. Based on the χ^2 minimization result, we computed the best age, or [age, $E(B - V)$] combination, and the uncertainty in the derived value from the χ^2 contours equal to minimum $(\chi^2) + 1$. We also computed the probability of the solution from each run to be the most appropriate one, given by a likelihood estimator of the form $p \sim \exp(-\chi^2)$. Of the 30 different estimates of ages and masses of each star cluster from our SED fitting analysis, we select final values with highest fitting probability. The typical uncertainty in age and mass is about 33 % across the whole sample, but smaller for younger clusters: 16 % for the subsample with ages < 1 Gyr, and 44 % for the older clusters. These errors are the formal uncertainties from the SED-fitting with best metallicity and extinction chosen in each case. We recall however, that for some of the photometry no errors were available and a constant uncertainty had

to be assumed for the whole catalog; in addition, the derived mass uncertainty takes into account the photometric errors and the derived [age, $E(B - V)$]: when the extinction is high, a larger uncertainty might affect the estimated mass. The scatter between age and mass values from the best SED-fitting solution (using the chosen metallicity and reddening) and values obtained with different assumptions, gives an indication of possible additional uncertainties. The difference between ages derived using models with solar, versus $Z=0.05$ metallicity, is $\leq 50\%$ at about 1 Gyr, $\leq 30\%$ at 100 Myr and much less for younger ages, higher metallicity yielding younger ages. The difference in resulting age using models with $Z=0.08$ versus solar metallicity is somewhat smaller, and between solutions with $Z=0.008$ versus $Z=0.004$ is much smaller. Precise estimates of metallicity from spectroscopy would be relevant to eliminate these factors of uncertainty.

We obtained results for 403, 185, and 57 objects from *FNugriz*, *FNUBVI*, and *FNugrizK*, respectively. In most cases, homogeneous optical bands (e.g., *ugriz* data) provided the best fits (see Figure 4). For 55 objects with measurements in less than three bands we do not estimate ages. The reddening values of 409 objects are adopted from the *indivEBV* and those of 236 objects are from the *freeEBV*. In Figure 7, we present the distribution of our estimated ages and masses of star clusters in M31. Comparison with young (≤ 1 Gyr; blue filled circles) and old (> 1 Gyr; red filled circles) star clusters obtained from Caldwell et al. (2009, 2011) shows that our estimations are consistent with their results. Finally, we obtained ages and masses of 176 young (≤ 1 Gyr) clusters and 446 old (> 1 Gyr) clusters from our analysis.

3.2. Comparison with Previous Results

In Figure 8, we compare our estimated ages of young clusters with results from previous works (e.g., Beasley et al. 2004; Puzia et al. 2005; Vansevičius et al. 2009; Wang et al.

2010; Fan et al. 2010; Perina et al. 2010; Caldwell et al. 2009, 2011). Beasley et al. (2004) estimated ages of 8 young clusters from a comparison of observed spectra with synthetic SSP models. Their ages are in good agreement with our estimations although there is a small (~ 0.1 Gyr) systematic offset. Vansevičius et al. (2009) estimated ages of star clusters located in the southern disk of M31 by multi-band (*UBVRI*) SED fitting. Our estimated ages of young clusters are similar to their results, albeit with some scatters. Puzia et al. (2005) compared the Lick indices to SSP models for their age estimation. Their ages show large discrepancy from ours. Since the SSP models which they used do not cover the age range less than 1 Gyr, the model limitation might be responsible for this discrepancy in young clusters. Perina et al. (2010) estimated ages of young clusters by comparing model isochrones with color-magnitude diagrams obtained from HST/WFPC2 observations. Their results are also in good agreement with ours. Wang et al. (2010) and Fan et al. (2010) estimated ages of clusters from multi-band SED fitting. Many of their estimated ages are largely discrepant from ours. Most of young clusters identified by them are in fact old and metal-poor (see also Caldwell et al. 2011). Caldwell et al. (2009, 2011) published ages of star clusters by comparing their high-quality integrated spectra with SSP models. Our age estimation for young clusters are in good agreement with results of Caldwell et al. (2009, 2011). It is worth to note that our age estimation based on SED fitting of multi-band photometry including UV data is comparable to those achieved by other works using spectroscopic line indices and color-magnitude diagrams. This emphasizes again that the UV photometry is a powerful tool for age estimation of young stellar populations (see also Kaviraj et al. 2007; Bianchi 2011).

In Figure 9, we also compare masses of young clusters from our analysis with other works: Beasley et al. (2004), Vansevičius et al. (2009), Perina et al. (2010), and Caldwell et al. (2009, 2011). In previous studies, masses are estimated from the mass-to-light ratio (M/L) coupled with estimated ages. Our estimated masses are slightly larger

than those of Beasley et al. (2004), Vansevičius et al. (2009), and Perina et al. (2010) by factors of 1.7, 1.8, and 1.6, respectively. However, our masses are in good agreement with estimations from Caldwell et al. (2009, 2011) (about 30 % higher, on average). Our young clusters have masses in the range of $\sim 3 \times 10^2 - 2 \times 10^5 M_{\odot}$.

3.3. Young Cluster Catalog

From our SED fitting analysis in Section 3.1, we select 176 young clusters younger than 1 Gyr, and confirm that their ages and masses are in good agreement with other previous results (see Section 3.2). For a complete list of young clusters, in addition to our sample, we also consider the 155 young clusters with ≤ 1 Gyr from Caldwell et al. (2009). Among our 176 young clusters, we only include 173; 129 objects are classified as young clusters in both of ours and Caldwell et al. (2009) analysis and for 44 clusters, ages were not estimated by Caldwell et al. (2009). We exclude three young clusters (B100, M019, PHF7-1) which have old (> 1 Gyr) ages in Caldwell et al. (2009). We add 9 young clusters which are only available in Caldwell et al. (2009) and adopted their ages and masses from Caldwell et al. (2009). We exclude 17 young clusters from Caldwell et al. (2009) which are estimated to be older than 1 Gyr by our analysis. Finally, we construct a final catalog of 182 young clusters consisting of our 173 young clusters and 9 young clusters from Caldwell et al. (2009). Table 2 presents a catalog of these young clusters with their ages and masses.

3.4. Color-Color and Color-Magnitude Diagrams

Figure 10 shows extinction-corrected $g - r$ vs. $UV - r$ (upper two panels) and $NUV - r$ vs. $FUV - r$ (lower right panel) diagrams for star clusters included in our catalog. Blue filled circles and red filled circles are young (≤ 1 Gyr) and old (> 1 Gyr) clusters, respectively.

The mean distribution of young clusters is biased towards blue colors in both optical and UV colors. The discrimination between young and old clusters is more prominent in the diagram $(\text{NUV}-r)_0$ vs. $(\text{FUV}-r)_0$, since UV fluxes are sensitive to the young stellar populations. The old GCs in the MW (crosses; Table 6 of Sohn et al. 2006) and the old clusters in M31 lay on the same locus in these diagrams. Different solid curves show Yonsei evolutionary population models in the age range 0.1 - 14 Gyr (from lower to upper: C. Chung et al. in preparation). The Galactic and M31 clusters follow the general trend indicated by the model lines.

In the $g-r$ vs. $\text{UV}-r$ diagrams, the dashed horizontal line corresponds to the reference value of $(g-r)_0 = 0.3$ for young cluster selection adopted by Peacock et al. (2010). The dashed vertical lines are also arbitrary reference values of $(\text{NUV}-r)_0 = 2.5$ and $(\text{FUV}-r)_0 = 3.0$ for young cluster selection (Bohlin et al. 1993; Rey et al. 2007). In the ranges of $(\text{NUV}-r)_0 < 2.5$ and $(\text{FUV}-r)_0 < 3.0$, the MW GC system lacks young clusters. Most of our young clusters have smaller values than the reference colors; $(g-r)_0 < 0.3$, $(\text{NUV}-r)_0 < 2.5$, and $(\text{FUV}-r)_0 < 3.0$. Fusi Pecci et al. (2005) selected massive young clusters in M31 according to their color and/or the strength of $\text{H}\beta$ spectral index with $\text{H}\beta > 3.5 \text{ \AA}$. In Figure 10, we also denote the clusters with $\text{H}\beta > 3.5 \text{ \AA}$ (open squares) compiled from Beasley et al. (2004), Fusi Pecci et al. (2005), and Galleti et al. (2009). It is clear that the distribution of $\text{H}\beta$ -selected sample is consistent with that of our young clusters. The lower left panel of Figure 10 shows the M_r vs. $\text{NUV}-r$ diagram for M31 clusters and MW GCs. A distance modulus of $(m-M)_0 = 24.47$ (McConnachie et al. 2005) was adopted for all M31 clusters. The most distinct feature is that young clusters with ≤ 1 Gyr are systematically fainter in V than the old clusters, which indicates that the M31 young clusters are systematically less massive objects than the old GCs in the M31 and the MW (see Section 4).

4. Properties of Young Clusters

4.1. Age and Mass Distribution

Figure 11 shows the distribution of estimated ages and masses for 182 young clusters. One interesting feature is that the majority of M31 clusters with age < 1 Gyr is rather biased towards the younger age range of < 500 Myr. In the age histogram (upper histogram), as the age of clusters decreases, the fraction of young clusters increases. About 82 % (149 of 182) of the clusters are younger than 500 Myr. Clusters older than 500 Myrs with mass lower than $\sim 10^4 M_{\odot}$ are too faint to be detected in the catalogs compiled in this work. However, even when we consider only clusters more massive than $10^4 M_{\odot}$, 73 % (73 out of 100) are younger than 500 Myrs. This may reflect effects of luminosity fading with age, cluster disruption, and possible variations in time of the cluster formation rate. On the other hand, most young clusters are in the mass range of $10^{3.5} - 10^{4.5} M_{\odot}$. The mean value of age and mass of young clusters is about 300 Myr and $10^4 M_{\odot}$, respectively. Note that, in the same age range, the mass distribution of our young clusters in M31 is similar to that of massive clusters found in the LMC and is in between those of Galactic young clusters and old GCs (Beasley et al. 2004; Fusi Pecci et al. 2005; Caldwell et al. 2009). In Figure 11, we also note that there is a general lack of massive young clusters with $> 10^5 M_{\odot}$ in M31.

Interestingly, many young clusters younger than 50 Myr are low mass ones with $< 10^{3.5} M_{\odot}$. Their masses are comparable to the mass range of typical MW open clusters (see Figure 14 of Caldwell et al. 2009). Even though there are a handful of young clusters with very low masses ($< 10^3 M_{\odot}$) and ages less than 10 Myr, it is obvious that our sample is not complete in detecting such faint and low mass clusters. Krienke & Hodge (2007) estimate that the entire disk of M31 contains approximately 80,000 such faint and small clusters extrapolating from their detected 343 clusters. Further deep HST observations for an extensive area of the M31 disk will clarify the nature of these low mass clusters and mass

distribution of cluster system in M31 (e.g., Panchromatic Hubble Andromeda Treasury (PHAT) survey, Johnson et al. 2011; Dalcanton et al. in preparation).

Young clusters are experiencing a serious loss of gas and dust during the supernovae explosion phase (10 - 50 Myr: Lada & Lada 2003; Fall et al. 2005; Goodwin 2009), internal dynamical evolution and stellar population fading (10 - 100 Myr: Lamers 2009), and galactic tidal effects and other external effects (100 - 1000 Myr: Boutloukos & Lamers 2003; Gieles et al. 2005; Lamers et al. 2005; Lamers & Gieles 2006; Gieles et al. 2007). Many low mass clusters can become gravitationally unbound and easy to disrupt within these phases (Pellerin et al. 2010). While survival of star clusters depends upon the mass, size, and environment, most low mass young clusters found in the M31 disk might be disrupted within few Gyrs.

4.2. Metallicity

Most previous results concerning the metallicity of star clusters in M31 were focused on old GCs. In our compiled catalog, metallicity values are available for 46 young clusters (see Section 2.2). As shown in Figure 12, young clusters appear to be biased towards the metal-poor range of $[\text{Fe}/\text{H}] < -1.0$. Our compiled metallicity values of 30 young clusters are from Perrett et al. (2002), eight values are the mean value from Perrett et al. (2002) and Barmby et al. (2000), four values are from Barmby et al. (2000), and the remaining four values are from Galleti et al. (2009). All of these metallicities are estimated from the Lick indices which were calibrated from the Galactic old GCs. On the other hand, Fusi Pecci et al. (2005) claimed that young clusters are probably not so metal-poor as deduced from the metallicity values provided by Perrett et al. (2002). From the specific comparison between $[\text{Fe}/\text{H}]$ values derived from different Lick indices, Fusi Pecci et al. (2005) concluded that G -band line strength tends to underestimate $[\text{Fe}/\text{H}]$ values in

Perrett et al. (2002) by more than 1 dex.

As a further argument, we compared metallicities of young clusters from our compiled catalog with other independent results from Beasley et al. (2004) and Perina et al. (2010). Beasley et al. (2004) obtained high-quality spectra for 8 young clusters and estimated their metallicities. Using HST/WFPC2 data, Perina et al. (2010) derived ages and metallicities of young cluster by fitting optical color-magnitude diagrams with theoretical isochrones. The $[\text{Fe}/\text{H}]$ values from Beasley et al. (2004) and Perina et al. (2010) are systematically higher (about 1.3 dex) than our compiled values. While the $[\text{Fe}/\text{H}]$ values of young clusters in our catalog mainly rely on the estimation of Perrett et al. (2002), we suggest these values might be underestimated. For completeness, in Table 1 ($[\text{Fe}/\text{H}]$ values in parenthesis of column (24)), we also include metallicity values of 34 young clusters from Beasley et al. (2004) and Perina et al. (2010).

In our SED fitting analysis, we used five discrete metallicity grids ($Z = 0.0004, 0.004, 0.008, 0.02, 0.05$) of SSP models. Although accurate metallicities cannot be derived from SED fitting, we can chose the model grid which provides the best fit, as an indication. In Figure 13, we compare our compiled $[\text{Fe}/\text{H}]$ with results from our SED fitting. Our $[\text{Fe}/\text{H}]$ values from SED fitting indicated by the best-probability solution (see Section 3.1) are systematically metal-rich with $[\text{Fe}/\text{H}] > -1.0$, and show large (more than 1 dex) differences with our compiled $[\text{Fe}/\text{H}]$. Consequently, we suggest that most young clusters in M31 might be more metal-rich, than the results from Perrett et al. (2002) indicate. We anticipate high precision spectroscopic observations for an extensive sample of young clusters in the future to clarify the metallicity distribution of young clusters.

4.3. Kinematics

Of the 617 compiled star clusters with measured radial velocity, the majority of the clusters are in the range of $-700 - 100 \text{ km s}^{-1}$. The mean value of radial velocity and velocity dispersion is -295 km s^{-1} and 163 km s^{-1} , respectively. This mean radial velocity is consistent with the known system velocity of M31, $V_{M31} = -301 \text{ km s}^{-1}$ (van den Bergh 2000), which we adopt in this paper.

In Figure 14, we present radial velocities of 617 star clusters, regardless of their ages, with respect to the system velocity of M31 against the projected distance along the major axis (black circles in left panels) and their velocity distribution (black histograms in right panels). We also divide the sample into star clusters which are located in different bins along the minor axis (i.e., different Y range) in order to inspect kinematical variation along the minor axis. In each left panel, a linear fit to the sample within $|X| = 10 \text{ kpc}$ (solid line), passing through $X = 0$ and $V_r - V_{M31} = 0$, along the major axis is also shown. The slope (α) of the linear fit decreases as the distance along the minor axis increases. It is evident from the figures that most of the star clusters in M31 show a sign of coherent rotation around the minor axis. The slope (α) of the linear fit in each bin along the minor axis is large and the velocity distributions have two peaks around the system velocity. This is in good agreement with previous results (e.g., Perrett et al. 2002; Lee et al. 2008). The rotation feature of the clusters at $|Y| < 3 \text{ kpc}$ is more evident compared with the counterparts at $|Y| > 3 \text{ kpc}$.

In Figure 14, we also present velocity distribution of old ($> 1 \text{ Gyr}$) clusters (red circles and red histograms). In both the whole old cluster sample and each subsample in different bins along the minor axis, a hint of rotation is also seen, but less prominent than in the whole sample. The clear rotation signature does not appear for the outermost clusters at $|Y| > 3 \text{ kpc}$. Furthermore, in each panel, large scatter around the linear fit is seen. These

indicate that, while the pressure support plays a significant role, rotational kinematics are also important for the old cluster system in M31. In the case of old clusters at $|Y| < 3$ kpc, they might be dominated by a central large bulge showing moderate rotation rather than by a pressure supported halo (see Lee et al. 2008 and references therein).

On the contrary, as shown in Figure 15, young (≤ 1 Gyr) star clusters show most striking feature of systematic rotation around the minor axis. The radial velocities of young clusters against the projected distance along the major axis show tight distribution with little scatters around the linear fit. This indicates that the system of young clusters is rotational supported in the M31 disk. The rotational velocity of young clusters at $|Y| < 1$ kpc is about 220 km s^{-1} .

Morrison et al. (2004) have suggested the existence of a cold thin-disk system of star clusters in M31. In order to further clarify the kinematics of young clusters, we attempt to select a subsystem of star clusters with thin-disk kinematics, therefore presumably associated with the disk of M31. Following Morrison et al. (2004), we considered a simple cold-disk kinematical model with zero-thickness. In this model, the position of a cluster in the disk is determined from its observed position on the sky. We use a rotation curve that is flat with $V_{\text{circular}} = 250 \text{ km s}^{-1}$ for $|R| > 6.5$ kpc and then falls linearly to zero at $X = 0$ (solid line in the bottom panel of Figure 16). We also adopt a distance to M31 of 785 kpc (McConnachie et al. 2005), system radial velocity of -301 km s^{-1} , inclination of 77.7 deg (van den Bergh 2000), and position angle of 37.7 deg (de Vaucouleurs 1958). If star clusters lay on the disk, we could calculate their velocities using our assumed cold-disk model and disk rotation curve. Finally, we measured the residual velocity which is defined as the absolute value of the difference between the calculated velocity and the actual observed velocity (see middle panel of Figure 16).

We split the star clusters into two subgroups according to their residual velocity:

thin-disk kinematics and non-thin-disk (i.e., bulge or halo) kinematics. We define thin-disk clusters as those with residual velocities less than 40 km s^{-1} (see dashed line in the middle panel of Figure 16) following the criterion of Morrison et al. (2004). About 90 % of the star clusters with thin-disk kinematics of Morrison et al. (2004) is recovered by our selection criteria. We divided 617 star clusters into 216 thin-disk clusters and 401 non-thin-disk clusters. In the case of old clusters, only 29 % of sample has thin-disk kinematics. On the other hand, 66 % of the young clusters (blue filled circles in Figure 16) shows thin-disk kinematics. Therefore, most young clusters (filled circles in Figure 16) have thin-disk kinematic characteristics (see also Fusi Pecci et al. 2005). This argument is also supported by the spatial distribution of young clusters, which are preferentially located along the 10 kpc ring (red ellipse in the top panel of Figure 16) in the disk of M31 (see also Section 4.4).

4.4. Spatial Distribution

In the top panel of Figure 16, we compare the spatial distribution of young ($\leq 1 \text{ Gyr}$, filled circles) and old ($> 1 \text{ Gyr}$, gray open circles) clusters in the plane of projected distances along the major (X) and minor (Y) axes. It is evident that old clusters are uniformly distributed all over M31 (from galaxy center to outermost disk regions), while many old clusters are concentrated near the central regions of M31 (i.e., bulge region). On the contrary, young clusters are lacking in the central regions of the galaxy and are evidently projected onto the disk between 5 kpc (inner dashed ellipse) and 18 kpc (outer dashed ellipse). Specifically, the spatial distribution of young clusters is well correlated with the well-known star-formation region associated with the 10 kpc “ring of fire” in the M31 disk (Brinks & Shane 1984; Dame et al. 1993; Pagani et al. 1999).

In Figure 17, we compare the spatial distribution of young clusters with respect to that

of OB stars (top panel), UV SF regions (middle panel), and dust (bottom panel). Young clusters in different age ranges (age < 100 Myr, 100 Myr < age < 400 Myr, and 400 Myr < age < 1 Gyr) are shown in different colors. We select O and B type stars (gray dots in the top panel) from *UBVRI* photometric data of Massey et al. (2006) (see Kang et al. 2009). We also consider 894 SF regions (gray contours in the middle panel) defined from the *GALEX* FUV imaging (Kang et al. 2009). The spatial distribution of dust from a *Spitzer* IRAC 8.0 μ m non-stellar image (Barmby et al. 2006) is also presented (contours in the bottom panel). The 10 kpc ring is approximated by a red ellipse. Evidently, the spatial distribution of young clusters correlate well with that of OB stars, UV SF regions, and dust as well as with the 10 kpc ring structure. However, it is noteworthy that the OB stars and UV SF regions spread out to the outer parts of the M31 disk, while young clusters are mostly confined to the regions around 10 kpc. There may be a selection effect favoring detection of UV SF regions and hot stars in the outer disk regions where extinction is less.

Figure 18 presents the number histogram of star clusters against the distance from the center of M31. OB stars and UV SF regions are also shown for comparison. A noticeable feature is that old clusters show a very different distribution from those of young clusters, OB stars, and UV SF regions. Old clusters are more centrally concentrated within ~ 10 kpc. While young clusters follow a similar distribution to OB stars and UV SF regions, young clusters show a peak around 10 kpc - 12 kpc. On the other hand, the distribution of OB stars and UV SF regions have an additional peak around 16 kpc. Consequently, we suggest that young clusters are closely correlated with OB stars and UV SF regions in their spatial distributions, although OB stars and UV SF regions show a more extended structure in the disk of M31. On the other hand, Azimlu et al. (2011) presented 3,691 HII regions on the disk of M31. They also found a reasonable spatial correlation between the luminous ($L_{H\alpha} > 10^{36} \text{ erg}^{-1}$) HII regions and young clusters (see Figure 9 of Azimlu et al. 2011).

4.5. Young Clusters and Star Formation Ring Structure

In Figure 19, we compare ages of young clusters (middle left panel) and UV SF regions (bottom left panel) against the de-projected distance from the center of M31. The overall young clusters distribution shows a single peak around 10 - 12 kpc. In addition to this main feature, a hint of small secondary peak is seen around 13 - 14 kpc. While young clusters in various age ranges within 1 Gyr contribute to the main peak, the small secondary peak might be ascribed to younger clusters with ages less than 400 Myr (see inset of the middle left panel). On the contrary, UV SF regions show two distinct peaks: a highest peak at ~ 16 kpc and a secondary peak around 11 kpc. The ages of most UV SF regions are younger than 400 Myr mostly due to our UV-based selection (Kang et al. 2009).

If young clusters are the result of active star formation in the M31 disk due to the head-on collision by a satellite galaxy, the age range of the majority of young clusters might be relevant to establishing the epoch of that event. Although the age distribution of our sample is somewhat broad, the majority of young clusters is in the age range of 100 - 400 Myr. Thus, our results appear to be consistent with the prediction by Block et al. (2006) of a collisional event with M32 about 210 Myr ago. Caldwell et al. (2009) claimed a possible spatial age variation among young clusters, considering models of recent interaction between M32 and the M31 disk and outward propagation of star burst through the disk by expanding density waves (Gordon et al. 2006; Block et al. 2006). We find no clear evidence of radial trend of cluster ages (see also Caldwell et al. 2009).

As shown in Figure 19 (middle right panel), most young clusters have masses between $10^{3.5}$ and $10^{4.5} M_{\odot}$. While there is no clear correlation between mass and radial distance, interestingly, young clusters located around 10 - 14 kpc have a wider mass range, compared with those in other regions. In this region, both high-mass ($> 10^{4.5} M_{\odot}$) and low-mass ($< 10^{3.5} M_{\odot}$) young clusters are found. The UV SF regions by Kang et al. (2009) have a mass

range wider than that of the young clusters and the majority have masses between 10^3 and $10^{5.5} M_{\odot}$. It is worth noting that more massive ($> 10^{5.5} M_{\odot}$) UV SF regions are also preferentially located at galactocentric distances around 10 - 14 kpc where massive young clusters are also found. Another group of massive UV SF regions is found around 5 kpc. On the contrary, low-mass UV SF regions are more numerous towards outer regions (> 10 kpc) of the M31 disk, and form a peak around 16 kpc. Based on the rarity of young clusters and systematically low-mass (and younger) UV SF regions outside 16 kpc, we suggest that the outer part of the disk of M31 has an environment insufficient to trigger formation of massive star clusters. This is also supported by the HI and CO surveys which show higher gas density around the 10 kpc ring and lower in outer parts (e.g., Brinks & Shane 1984; Dame et al. 1993; Nieten et al. 2006).

Using *Spitzer* MIPS images, Gordon et al. (2006) suggested that the morphology of the dust in M31 is well represented by a composite of two logarithmic spiral arms and a 10 kpc circular star forming ring offset from the nucleus. Following the approach of Gordon et al. (2006), in Figure 20 we examine the spatial arrangement of UV SF regions and young clusters. In the upper panels, the black large circle is the 10 kpc star formation ring, offset from the center of M31 by (4.5 kpc, 1.0 kpc) and with a radius of 44 arcmin (10 kpc). The two gray spirals are simple logarithmic spirals adopted from Gordon et al. (2006). Most UV SF regions do not follow the two spiral arms and show deviations from the spiral pattern, while some UV SF regions in the inner disk (inside 10 kpc) appear to roughly follow two logarithmic spirals. The distribution of many UV SF regions is well fitted by a 10 kpc circle. The UV SF regions in the outer disk (outside 12 kpc) present several arcs rather than spiral arms pattern. The distribution of young clusters is more distinct and simple; most young clusters are around the 10 kpc circular ring, while two spirals trace a handful of young clusters inside the 10 kpc ring. To confirm the distribution of UV SF regions and young clusters around the 10 kpc ring, in the lower panel of Figure 20

we present their spatial distribution in polar coordinates. The position angle is defined to be increasing clockwise starting from northeast (NE) in the upper panels of Figure 20. The most interesting feature is the wavy distribution of SF regions and young clusters fitted by a black solid curve, representing the ~ 10 kpc ring, except for the region around 220 deg where the ring splits. This wavy line is characterized by parameters of the circle shown in the upper panels of Figure 20. This wavy feature is more distinct in the case of young clusters (colored filled circles). Consequently, we confirm that the distribution of young clusters and UV SF regions in the M31 disk is consistent with a circular star formation ring with radius ~ 10 kpc in combination with simple logarithmic spirals.

Another thing to be noted in Figure 20 is an asymmetric number distribution of young clusters with position angle. The number (125) of young clusters in the southern disk of M31 (from 180 to 360 degree) is larger than that (57) of young clusters in the northern disk (from 0 to 180 degree). Fan et al. (2008) noted that the highly extinguished star clusters with $E(B - V) > 0.4$ mag are preferentially located on the northwestern (NW) side (see also Figure 17 of Caldwell et al. 2011). If the difference is entirely due to the reddening being higher on the NW half, the frequency and distribution of young clusters in the northern disk based on currently available catalogs remains to be updated from extensive and deeper observations in future.

4.6. Ring Splitting Region and Compact Star Clusters

A prominent feature in the southern part of the M31 disk is the region of ring split. In the distribution of both Kang et al. (2009) UV SF regions and our young clusters, a hole that matches the observed split in the ring near M32 is seen around $X = -8$ kpc and $Y = 8$ kpc (upper panels in Figure 20) and position angle $\sim 160 - 270$ deg (lower panel in Figure 20). This was discovered by Gordon et al. (2006) from the IR-emitting dust distribution,

and they suggested that the split of the ring in the form of a hole is caused by a passage of M32 through the M31 disk (see also Block et al. 2006). Many UV SF regions and young clusters are located outside of the ring splitting. As shown in the lower panel of Figure 20 (histogram of position angle), young clusters and SF regions show distinct peaks around 180 and 240 deg. These peaks appear to be constituted mostly of clusters younger than 400 Myr.

Recently, based on high-resolution SUBARU Suprime-Cam images, Vansevičius et al. (2009) carried out a survey of compact star clusters in the southwestern part of the M31 disk including the ring splitting region. The apparent size of these compact clusters is less than 3 arcsec and for most sample it is smaller (< 2.5 pc) than typical MW GCs. They estimated ages and masses of 238 high-probability star clusters based on the *UBVRI* photometry from the LGGS images. These star clusters are mainly selected by specifying a lower limit of half-light radius ($r_h \gtrsim 0.15$ arcsec or $\gtrsim 0.6$ pc, see Vansevičius et al. (2009) for the details). The majority of their compact clusters are young objects, with ages less than 1 Gyr (186 of 238) and a peak around 70 Myr. They span a mass range of $10^{2.0}$ - $10^{4.3} M_\odot$ peaking at $\sim 4 \times 10^3 M_\odot$.

In Figure 21, we present age and mass distribution of our young clusters (black filled and open circles) and 186 compact star clusters (gray filled circles) younger than 1 Gyr from Vansevičius et al. (2009). While the overall distribution of our young clusters is consistent with that of Vansevičius et al. (2009) compact star clusters, it is obvious that Vansevičius et al. (2009) detected more objects in the lower mass ($< 10^{3.5} M_\odot$) and younger age (< 100 Myr) ranges. About half (95) of their sample clusters are younger than 100 Myr. In their sample, there is a lack of relatively massive ($> 10^4 M_\odot$) compact clusters with ages 400 Myr - 1 Gyr. Young clusters included in our compiled catalog show systematically higher mass (see mass histogram of Figure 21) than the cluster sample of Vansevičius et al.

(2009), probably due to the brighter limit of cluster selection used in previous literature.

In Figure 22, we present the spatial distribution of 186 compact star clusters (filled circles) with ages younger than 1 Gyr from Vansevičius et al. (2009) along with our young clusters (open circles). The clusters are divided into two age groups: younger than 100 Myr (blue) and 100 Myr - 1 Gyr (red). We also overplot the distributions of dust from *Spitzer* IRAC 8.0 μm image (gray contours) and UV SF regions (orange contours). The distribution of clusters younger than 100 Myr follows well that of dust and UV SF regions. Furthermore, as noted by Vansevičius et al. (2009), two clumps of young clusters are found at $(X, Y) \sim (-10.2 \text{ kpc}, -2.2 \text{ kpc})$ and $(-10.5 \text{ kpc}, -0.5 \text{ kpc})$. On the other hand, relatively older ($> 100 \text{ Myr}$) clusters are widely distributed over the area. Older ($> 100 \text{ Myr}$) clusters are preferentially located in the gap of the ring splitting area (e.g., $-9.5 \text{ kpc} < X < -7 \text{ kpc}$ and $-2.5 \text{ kpc} < Y < -0.5 \text{ kpc}$) where dust and UV SF regions lack. Regarding the scenario whereby the passage of M32 through the M31 disk triggered a burst of star formation (Gordon et al. 2006), we speculate that older ($> 100 \text{ Myr}$) clusters in the ring splitting hole were formed at the epoch of the first passage of M32, while formation of younger ($< 100 \text{ Myr}$) clusters around the hole region might be induced by later shock propagation.

5. Summary and Conclusion

We constructed a comprehensive star cluster catalog which contains 700 M31 star clusters compiled from RBC v4 (Galleti et al. 2004), Caldwell et al. (2009, 2011), and Peacock et al. (2010). We detected 418 and 257 clusters in *GALEX* NUV and FUV, respectively, above flux limits of 23.7 and 23.6 ABmags and measured their UV magnitudes. Our catalog includes photometry in up to 16 passbands ranging from FUV to NIR as well as ancillary information such as reddening, metallicity, and radial velocities. Our merged catalog is the most extensive and updated one of UV photometry for M31 star clusters,

superseding our previous UV catalog (Rey et al. 2007). We estimated ages and masses of star clusters by multi-band SED fitting; the UV photometry enables more accurate age estimation of young clusters.

We also extracted a sample of 182 young clusters with ages less than 1 Gyr consisting of 173 clusters with our age estimation and 9 clusters from Caldwell et al. (2009). Our estimated ages and masses of young clusters are in good agreement with previous literature (e.g., Beasley et al. 2004; Caldwell et al. 2009; Vansevičius et al. 2009; Perina et al. 2010). We examined the properties of young clusters such as age and mass distribution, metallicity, kinematics, and spatial distribution which provide unique probes of the star formation history of the disk of M31, and the prominent 10 kpc ring structure in particular. The mean age and mass of the young clusters are about 300 Myr and $10^4 M_{\odot}$, respectively. The mass range of our young clusters in M31 is similar to that of massive clusters found in the LMC and is in between those of Galactic young clusters and old GCs (Beasley et al. 2004; Fusi Pecci et al. 2005; Caldwell et al. 2009). Since most low-mass ($< 10^5 M_{\odot}$) clusters are young objects, we consider they may be disrupted within a few Gyrs (Lamers et al. 2005).

The $[\text{Fe}/\text{H}]$ values of young clusters included in our catalog, which are mostly from Perrett et al. (2002), are systematically lower (by more than 1 dex) than those derived from high-quality spectroscopic data or inferred from our SED fitting. While high precision spectroscopic observations for an extensive sample of young clusters are anticipated, we suggest that most young clusters in M31 might have moderately enhanced metallicity (i.e., $[\text{Fe}/\text{H}] > -1.0$). Such a high metallicity of the M31 disk and associated young clusters is consistent with the general result that spiral’s stellar disk is metal-rich (Bell & de Jong 2000), when not experiencing substantial gas infall or outflow (e.g., Dalcanton 2007).

By comparing radial velocities of star clusters with a cold disk model, we selected a subsystem of star clusters with thin-disk kinematics, associated with the disk of M31. We

confirm that most of the young clusters show systematic rotation around the minor axis and are kinematically associated with the thin-disk of M31. The majority of young clusters is located between 5 and 18 kpc from the center of M31 and shows a distinct peak around 10 - 12 kpc. The distribution of young clusters is closely correlated with that of other tracers of disk structure (OB stars, UV SF regions, and dust).

Considering their kinematical properties and spatial distribution, young clusters are well correlated with the 10 kpc ring structure in M31. This structure, known as the ring of fire or star-formation ring, is off-centered from the galaxy nucleus (Block et al. 2006 and references therein). Block et al. (2006) discovered an inner dust ring, offset from the center of M31, and suggested that the two rings originated from a recent passage of a satellite. By numerical simulations, Block et al. (2006) inferred that the star formation ring structure results from a head-on collision through the center of the disk of M31 by a companion satellite galaxy. This event can produce density wave rings which triggered massive star formation at the peak of the wave. They postulated a recent (about 210 Myr ago) interaction between M32 and the M31 disk. We confirm that the spatial distribution of young clusters in the M31 disk is well re-presented by a circular 10 kpc star formation ring. Although the age distribution of our sample is somewhat broad, the majority of young clusters is in the age range of 100 - 400 Myr, which appear to be consistent with the prediction of Block et al. (2006). Therefore, we speculate that a large fraction of young clusters found in the M31 disk might have formed during the recent interaction between a satellite galaxy and the M31 disk, in which the star formation ring also originated. In particular, there is a split of the ring structure in the southern part of the M31 disk which corresponds to a gap in both IR contours and UV SF regions. Young clusters also show concentration outside the ring splitting and, furthermore, most of them have systematically younger (< 100 Myr) ages. Some young clusters in this region might derive from another interaction with a satellite galaxy, related with the Southern Stream emerging from the

southwest disk of M31 (Lee et al. 2008).

Within the context of merger history of M31, it is not unreasonable that the star formation ring in M31 has been shaped by a recent collision of satellite accompanied by higher star formation rate than that of the MW (Renda et al. 2005; Yin et al. 2009). Due to a recent major perturbation of the M31 disk, formation of significant young stellar populations and massive young clusters is expected. Low-level star formation (e.g., in quiescent galactic disks) tends to produce few, if any, massive young clusters. It is worth noting that M31 appears to be representative of the typical population of local spiral galaxies showing evidence of merging in the formation and evolution history (e.g., Hammer et al. 2007). On the other hand, the MW is a rather quiescent galaxy without any major interaction over the past few billion years. In this case, the MW disk may have evolved with a secular pattern (e.g., smooth gas accretion or infall; Croton et al. 2006; Hammer et al. 2007) without any violent merging event. This kind of quiescent environment of the Galactic disk can support the nonexistence of the populous massive young clusters found in M31. On the other hand, although head-on collisions between galaxies are rare (see Madore et al. 2009), M31 serves as an important local template, to understand more distant collisional ring galaxies (Moiseev & Bizyaev 2009 and references therein).

We are grateful to P. Barmby for kindly providing the *Spitzer* IRAC image. The authors would like to thank the anonymous referee for thoughtful comments that helped to improved this paper. The *GALEX* data presented in this paper were obtained from the Multimission Archive at the Space Telescope Science Institute (MAST). This research was supported by Basic Science Research Program through the National Research Foundation of Korea (NRF) funded by the Ministry of Education, Science and Technology (No. 2009-0070263). Support for this work was also provided by the NRF of Korea to the Center for Galaxy Evolution Research. *GALEX* (Galaxy Evolution Explorer) is a NASA

Small Explorer, launched in April 2003. We gratefully acknowledge NASA’s support for construction, operation, and science analysis of the *GALEX* mission, developed in cooperation with the Centre National d’Etudes Spatiales of France and the Korean Ministry of Science and Technology.

REFERENCES

- Alves-Brito, A., Forbes, D. A., Mendel, J. T., Hau, G. K. T., & Murphy, M. T. 2009, MNRAS, 395, L34
- Anders, P., Bissantz, N., Fritze-v. Alvensleben, U., & de Grijs, R. 2004, MNRAS, 347, 196
- Azimlu, M., Marciniak, R., & Barmby, P. 2011, AJ, 142, 139
- Barmby, P., Huchra, J. P., Brodie, J. P., et al. 2000, AJ, 119, 727
- Barmby, P., Ashby, M. L. N., Bianchi, L., et al. 2006, ApJ, 650, L45
- Barmby, P., Perina, S., Bellazzini, M., et al. 2009, AJ, 138, 1667
- Beasley, M. A., Brodie, J. P., Strader, J., et al. 2004, AJ, 128, 1623
- Beasley, M. A., Brodie, J. P., Strader, J., et al. 2005, AJ, 129, 1412
- Bell, E. F., & de Jong, R. S. 2000, MNRAS, 312, 497
- Bianchi, L., Clayton, G. C., Bohlin, R. C., Hutchings, J. B., & Massey, P. 1996, ApJ, 471, 203
- Bianchi, L. 2009, Ap&SS, 320, 11
- Bianchi, L. 2011, Ap&SS, 335, 51
- Block, D. L., Bournaud, F., Combes, F., et al. 2006, Nature, 443, 832
- Bohlin, R. C., Deutsch, E. W., McQuade, K. A., et al. 1993, ApJ, 417, 127
- Boutloukos, S. G., & Lamers, H. J. G. L. M. 2003, MNRAS, 338, 717
- Brinks, E., & Shane, W. W. 1984, A&AS, 55, 179

- Brodie, J. P., & Strader, J. 2006, *ARA&A*, 44, 193
- Brown, T. M., Smith, E., Ferguson, H. C., et al. 2006, *ApJ*, 652, 323
- Burstein, D., Li, Y., Freeman, K. C., et al. 2004, *ApJ*, 614, 158
- Caldwell, N., Harding, P., Morrison, H., et al. 2009, *AJ*, 137, 94
- Caldwell, N., Schiavon, R., Morrison, H., Rose, J. A., & Harding, P. 2011, *AJ*, 141, 61
- Croton, D. J., Springel, V., White, S. D. M., et al. 2006, *MNRAS*, 365, 11
- Dalcanton, J. J. 2007, *ApJ*, 658, 941
- Dame, T. M., Koper, E., Israel, F. P., & Thaddeus, P. 1993, *ApJ*, 418, 730
- de Grijs, R., Fritze-v. Alvensleben, U., Anders, P., et al. 2003, *MNRAS*, 342, 259
- de Vaucouleurs, G. 1958, *ApJ*, 128, 465
- Fall, S. M., Chandar, R., & Whitmore, B. C. 2005, *ApJ*, 631, L133
- Fan, Z., Ma, J., de Grijs, R., & Zhou, X. 2008, *MNRAS*, 385, 1973
- Fan, Z., de Grijs, R., & Zhou, X. 2010, *ApJ*, 725, 200
- Fusi Pecci, F., Bellazzini, M., Buzzoni, A., De Simone, E., & Federici, L. 2005, *AJ*, 130, 554
- Galleti, S., Federici, L., Bellazzini, M., Fusi Pecci, F., & Macrina, S. 2004, *A&A*, 416, 917
- Galleti, S., Federici, L., Bellazzini, M., Buzzoni, A., & Fusi Pecci, F. 2006, *A&A*, 456, 985
- Galleti, S., Bellazzini, L., Buzzoni, M., Federici, A., & Fusi Pecci, F. 2009, *A&A*, 471, 127
- Gieles, M., Bastian, N., Lamers, H. J. G. L. M., & Mout, J. N. 2005, *A&A*, 441, 949
- Gieles, M., Athanassoula, E., & Portegies Zwart, S. F. 2007, *MNRAS*, 376, 809

- Goodwin, S. P. 2009, *Ap&SS*, 324, 259
- Gordon, K. D., Bailin, J., Engelbracht, C. W., et al. 2006, *ApJ*, 638, L87
- Hammer, F., Puech, M., Chemin, L., Flores, H., & Lehnert, M. D. 2007, *ApJ*, 662, 322
- Huchra, J. P., Brodie, J. P., & Kent, S. M. 1991, *ApJ*, 370, 495
- Huxor, A. P., Tanvir, N. R., Ferguson, A. M. N., et al. 2008, *MNRAS*, 385, 1989
- Ibata, R., Irwin, M., Lewis, G., Ferguson, A. M. N., & Tanvir, N. 2001, *Nature*, 412, 49
- Ibata, R., Martin, N. F., Irwin, M., et al. 2007, *ApJ*, 671, 1591
- Johnson, L. C., Seth, A. C., Dalcanton, J. J., et al. 2011, *arXiv:1107.2668*
- Kang, Y., Bianchi, L., & Rey, S.-C. 2009, *ApJ*, 703, 614
- Karachentsev, I. D., Karachentseva, V. E., Huchtmeier, W. K., & Makarov, D. I. 2004, *AJ*, 127, 2031
- Kaviraj, S., Rey, S.-C., Rich, R. M., Yoon, S.-J., & Yi, S. K. 2007, *MNRAS*, 381, L74
- Kim, S. C., Lee, M. G., Geisler, D., et al. 2007, *AJ*, 134, 706
- Krienke, O. K., & Hodge, P. W. 2007, *PASP*, 119, 7
- Lada, C. J., & Lada, E. A. 2003, *ARA&A*, 41, 57
- Lamers, H. J. G. L. M., Gieles, M., Bastian, N., et al. 2005, *A&A*, 441, 117
- Lamers, H. J. G. L. M., & Gieles, M. 2006, *A&A*, 455, L17
- Lamers, H. J. G. L. M. 2009, *Ap&SS*, 324, 183
- Larsen, S. S., & Richtler, T. 2000, *A&A*, 354, 836

- Lee, M. G., Hwang, H. S., Kim, S. C., et al. 2008, *ApJ*, 674, 886
- Madore, B. F., Nelson, E., & Petrillo, K. 2009, *ApJS*, 181, 572
- Massey, P. 2003, *ARA&A*, 41, 15
- Massey, P., Olsen, K. A. G., Hodge, P. W., et al. 2006, *AJ*, 131, 2478
- McConnachie, A. W., Irwin, M. J., Ferguson, A. M. N., et al. 2005, *MNRAS*, 356, 979
- McConnachie, A. W., Irwin, M. J., Ibata, R. A., et al. 2009, *Nature*, 461, 66
- Messineo, M., Davies, B., Ivanov, V. D., et al. 2009, *ApJ*, 697, 701
- Moiseev, A. V., & Bizyaev, D. V. 2009, *New A Rev.*, 53, 169
- Mori, M., & Rich, R. M. 2008, *ApJ*, 674, L77
- Morrissey, P., Conrow, T., Barlow, T. A., et al. 2007, *ApJS*, 173, 682
- Morrison, H. L., Harding, P., Perrett, K., & Hurley-Keller, D. 2004, *ApJ*, 603, 87
- Nieten, C., Neininger, N., Guélin, M., et al. 2006, *A&A*, 453, 459
- Pagani, L., Lequeux, J., Cesarsky, D., et al. 1999, *A&A*, 351, 447
- Peacock, M. B., Maccarone, T. J., Knigge, C., et al. 2010, *MNRAS*, 402, 803
- Pellerin, A., Meurer, G. R., Bekki, K., et al. 2010, *AJ*, 139, 1369
- Perina, S., Cohen, J. G., Barmby, P., et al. 2010, *A&A*, 511, A23
- Perrett, K. M., Bridges, T. J., Hanes, D. A., et al. 2002, *AJ*, 123, 2490
- Puzia, T. H., Perrett, K. M., & Bridges, T. J. 2005, *A&A*, 434, 909
- Renda, A., Kawata, D., Fenner, Y., & Gibson, B. K. 2005, *MNRAS*, 356, 1071

- Rey, S.-C., Rich, R. M., Lee, Y.-W., et al. 2005, *ApJ*, 619, L119
- Rey, S.-C., Rich, R. M., Sohn, S. T., et al. 2007, *ApJS*, 173, 643
- Salpeter, E. E. 1955, *ApJ*, 121, 161
- Sohn, S. T., O’Connell, R. W., Kundu, A., et al. 2006, *AJ*, 131, 866
- Springel, V., White, S. D. M., Jenkins, A., et al. 2005, *Nature*, 435, 629
- Stetson, P. B. 1987, *PASP*, 99, 191
- van den Bergh, S. 2000, *The Galaxies of the Local Group*, Cambridge Astrophysics Series, Vol. 35 (Cambridge; Cambridge Univ. Press)
- Vansevičius, V., Kodaira, K., Narbutis, D., et al. 2009, *ApJ*, 703, 1872
- Wang, S., Fan, Z., Ma, J., de Grijs, R., & Zhou, X. 2010, *AJ*, 139, 1438
- White, S. D. M., & Rees, M. J. 1978, *MNRAS*, 183, 341
- White, S. D. M., & Frenk, C. S. 1991, *ApJ*, 379, 52
- Yin, J., Hou, J. L., Prantzos, N., et al. 2009, *A&A*, 505, 497

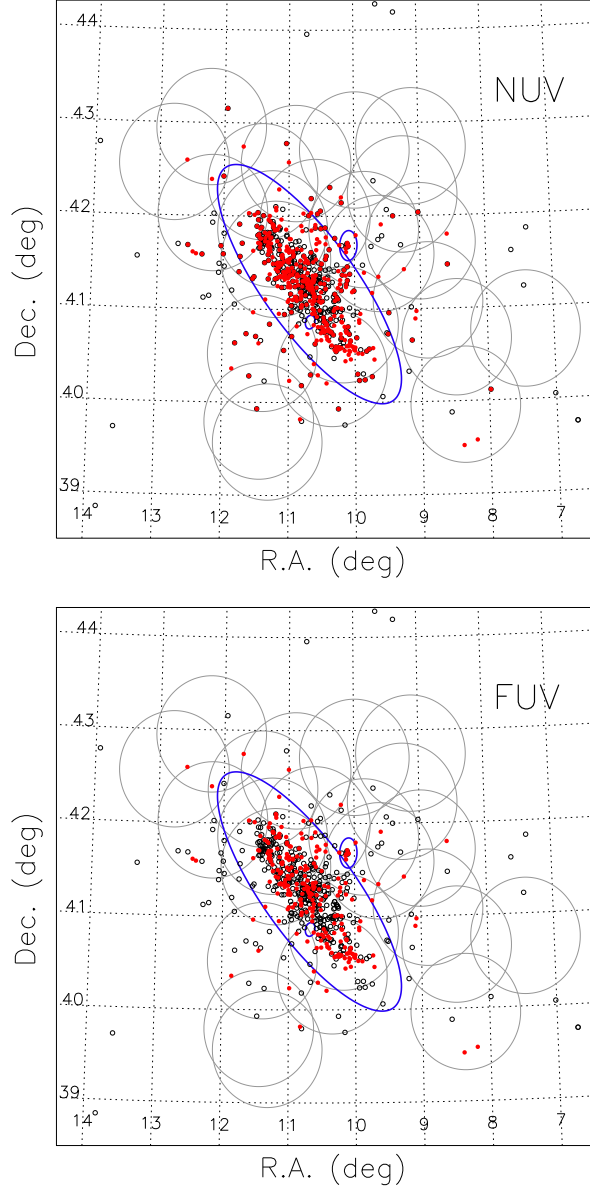


Fig. 1.— Spatial distribution on the sky of star clusters detected in *GALEX* NUV (*top panel*) and FUV (*bottom panel*) fields. Of the 700 star clusters, red filled circles are UV detected ones and black open circles are those not detected in UV. The large blue ellipse is M31 and two smaller ellipses are NGC 205 (*larger ellipse*) and M32 (*smaller ellipse*) with the D_{25} isophotes (Karachentsev et al. 2004). Gray circles are 23 *GALEX* fields.

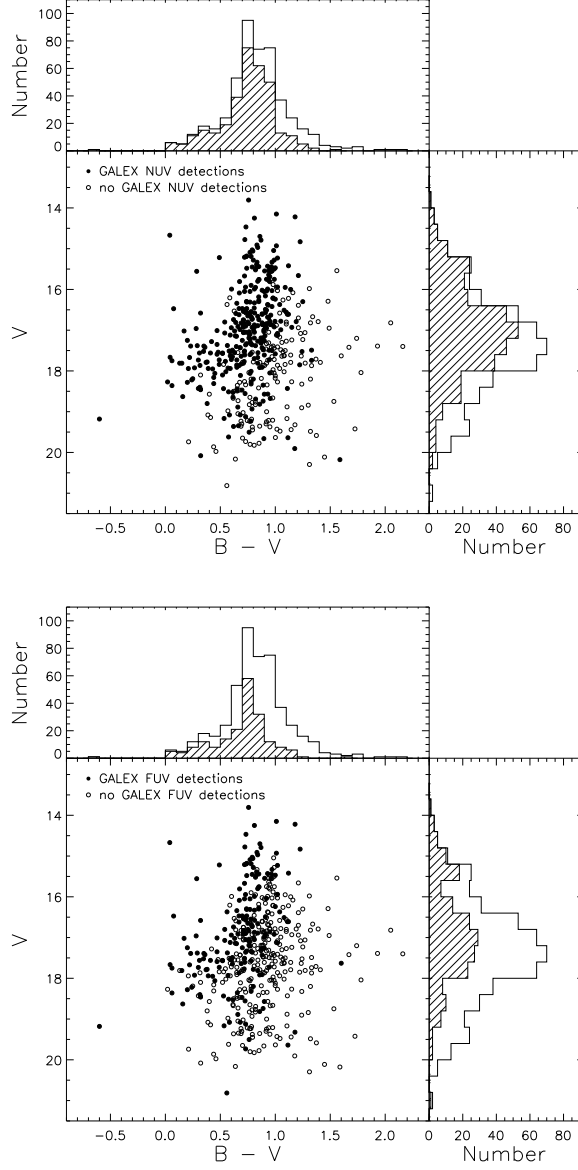


Fig. 2.— *GALEX* detection rates in NUV (*top panel*) and FUV (*bottom panel*). Of the 484 clusters with both B and V data, 328 (about 68 %) and 191 (about 39 %) clusters are detected in the *GALEX* NUV and FUV, respectively.

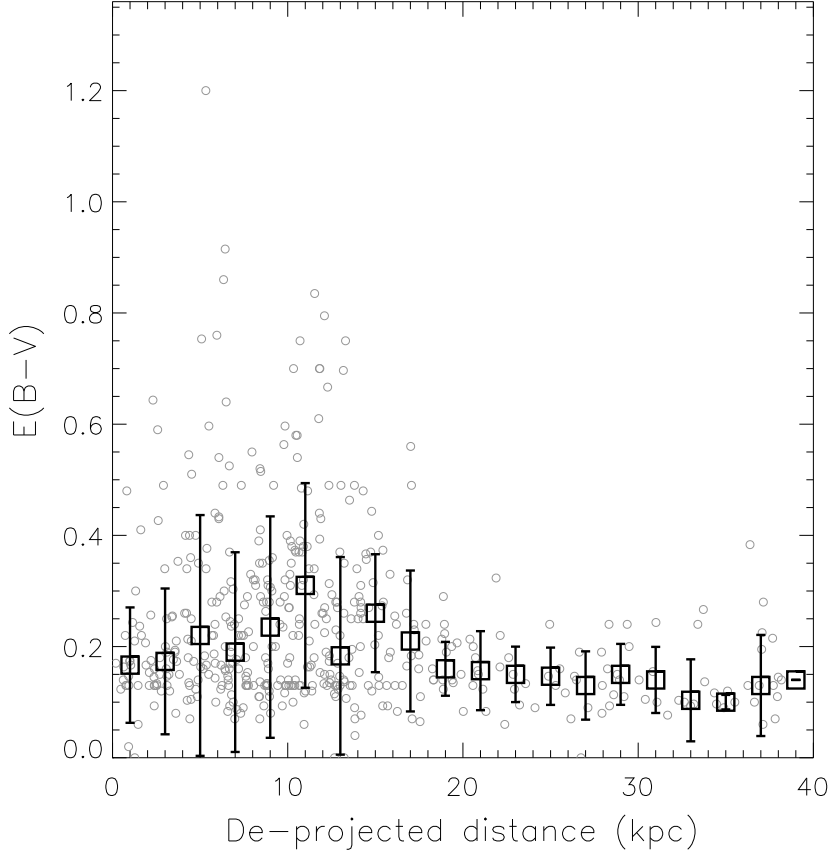


Fig. 3.— Distribution of our compiled reddening values of 555 star clusters (open circles) against their de-projected distances from the center of M31. Squares and error bars are median reddening values and standard deviations of star clusters located within annuli at every 2 kpc from the center of M31. The NW half of the disk has higher $E(B - V)$ on average than the SE region but the difference is less than respective standard deviations.

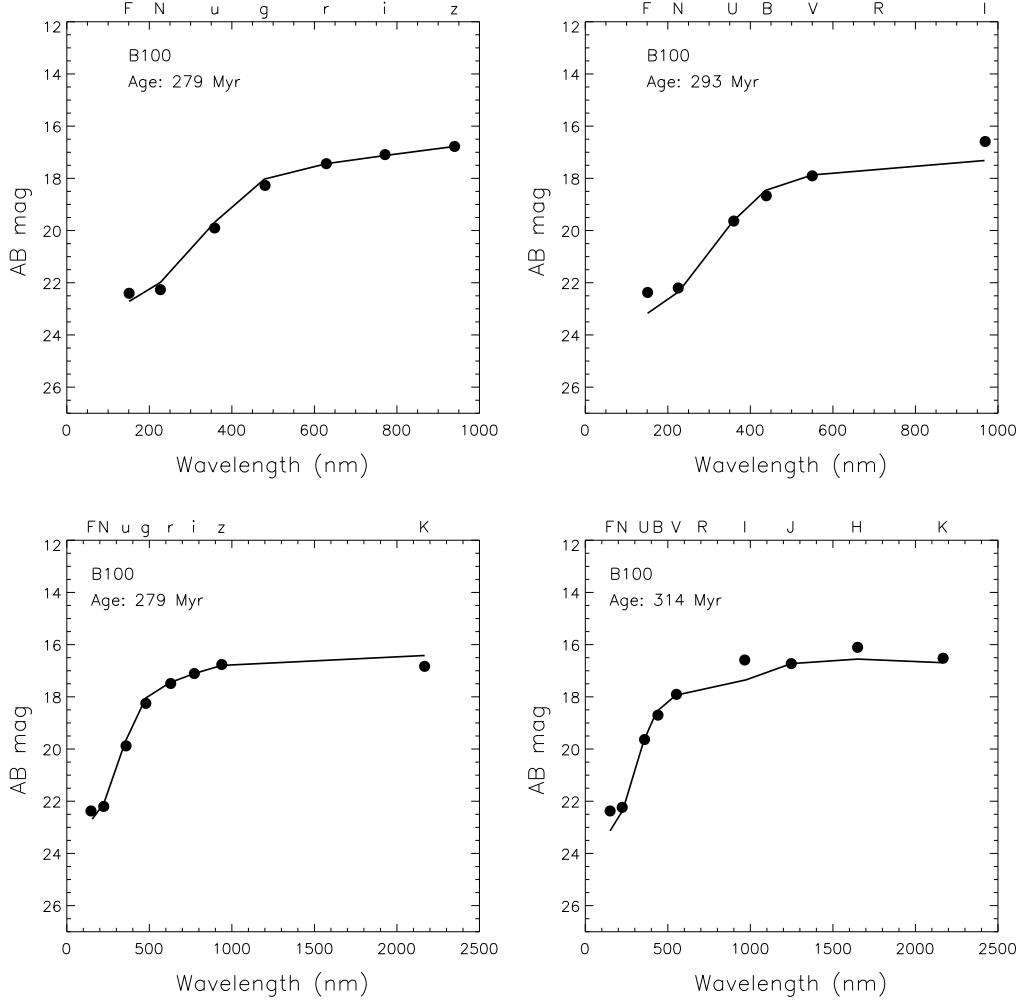


Fig. 4.— Examples of SED fitting for *FNugriz*, *FNUBVRI*, *FNugrizK*, and *FNUBVRIJHK* photometry. Filled circles are photometric measurements at different pass-bands in AB mag system. The object name and the estimated age are indicated in the left upper corner of each panel. Reddening values are adopted from our compiled catalog.

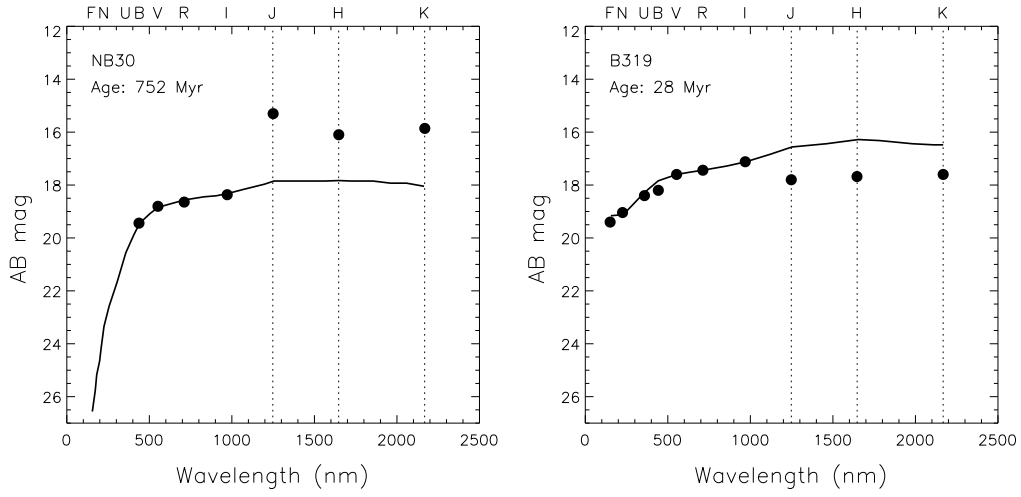


Fig. 5.— Examples of SED fitting for FUV, NUV, $UBVRI$, where the JHK photometry is inconsistent. Filled circles are photometric measurements at different passbands in AB mag system. Vertical dotted lines indicate JHK bands. The object name and the estimated age are indicated in the left upper corner of each panel. Reddening values are adopted from our compiled catalog. The photometry in JHK bands shows large discrepancies by > 1 mag from UV and optical bands regardless of the adopted best-fit model.

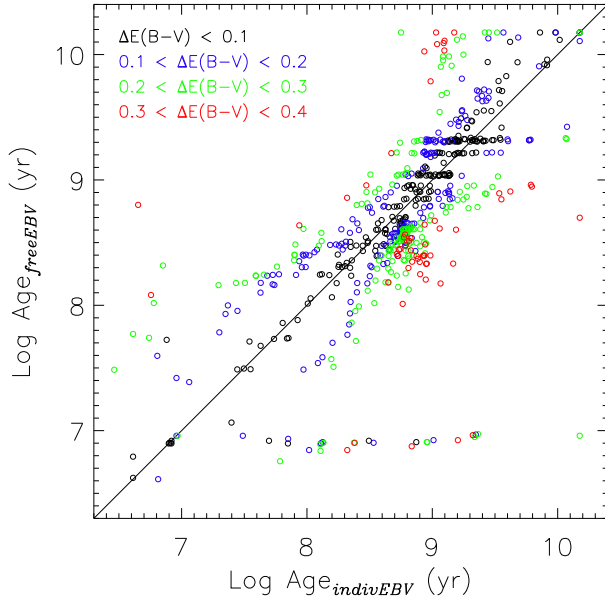


Fig. 6.— Comparison of ages derived from SED-fitting (1) imposing the $E(B-V)$ values from literature (*indivEBV*, X axis) and (2) treating $E(B-V)$ as a free parameter (*freeEBV*, Y axis). The symbols are color-coded according to the difference between *indivEBV* and *freeEBV* in the four cases: black ($\Delta E(B-V) < 0.1$), blue ($0.1 < \Delta E(B-V) < 0.2$), green ($0.2 < \Delta E(B-V) < 0.3$), and red ($0.3 < \Delta E(B-V) < 0.4$). The example shows results from the *FNugriz* dataset, analyzed with $Z=0.02$ metallicity models.

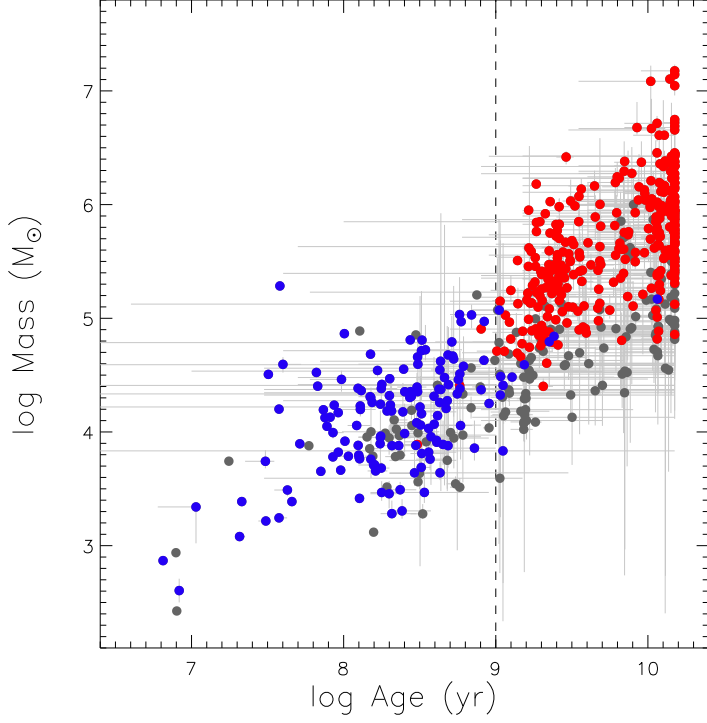


Fig. 7.— Distribution of estimated age and mass of star clusters in M31 from SED fitting. Blue filled circles are star clusters younger than 1 Gyr and red filled circles are those older than 1 Gyr according to the age estimated by Caldwell et al. (2009, 2011). Gray filled circles are clusters with no age estimates from Caldwell et al. (2009, 2011). Vertical dashed line indicates 1 Gyr. Error bars are uncertainties in the estimated ages and masses from χ^2 contours which are equal to minimum (χ^2) + 1.

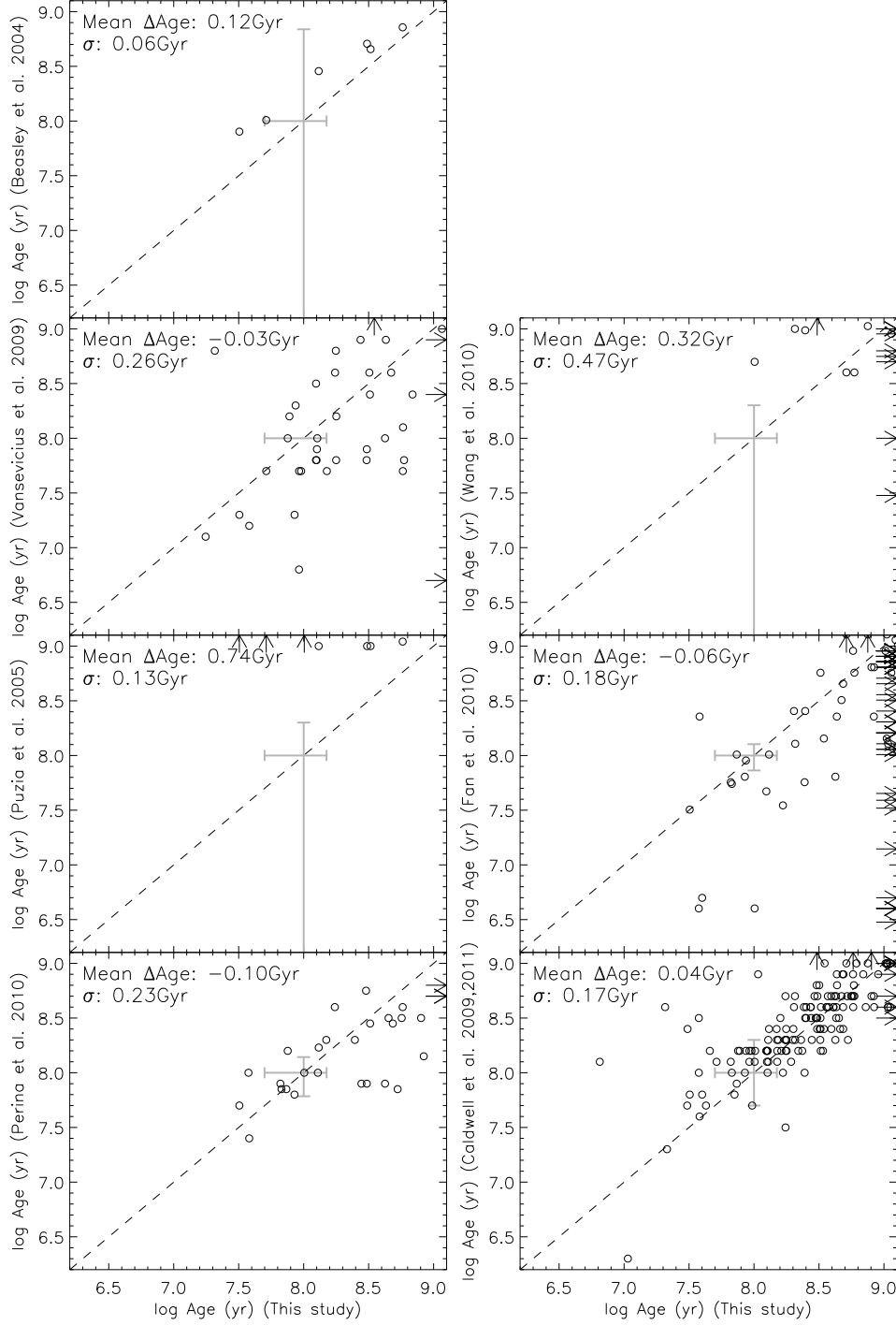


Fig. 8.— Comparison between age from our analysis and other studies for young clusters: Beasley et al. (2004), Vansevičius et al. (2009), Puzia et al. (2005), Perina et al. (2010), Wang et al. (2010), Fan et al. (2010), and Caldwell et al. (2009, 2011). In each plot, the mean value of the age difference (other study minus ours) is given, with its standard deviation (σ). Error bars show median errors of cluster ages.

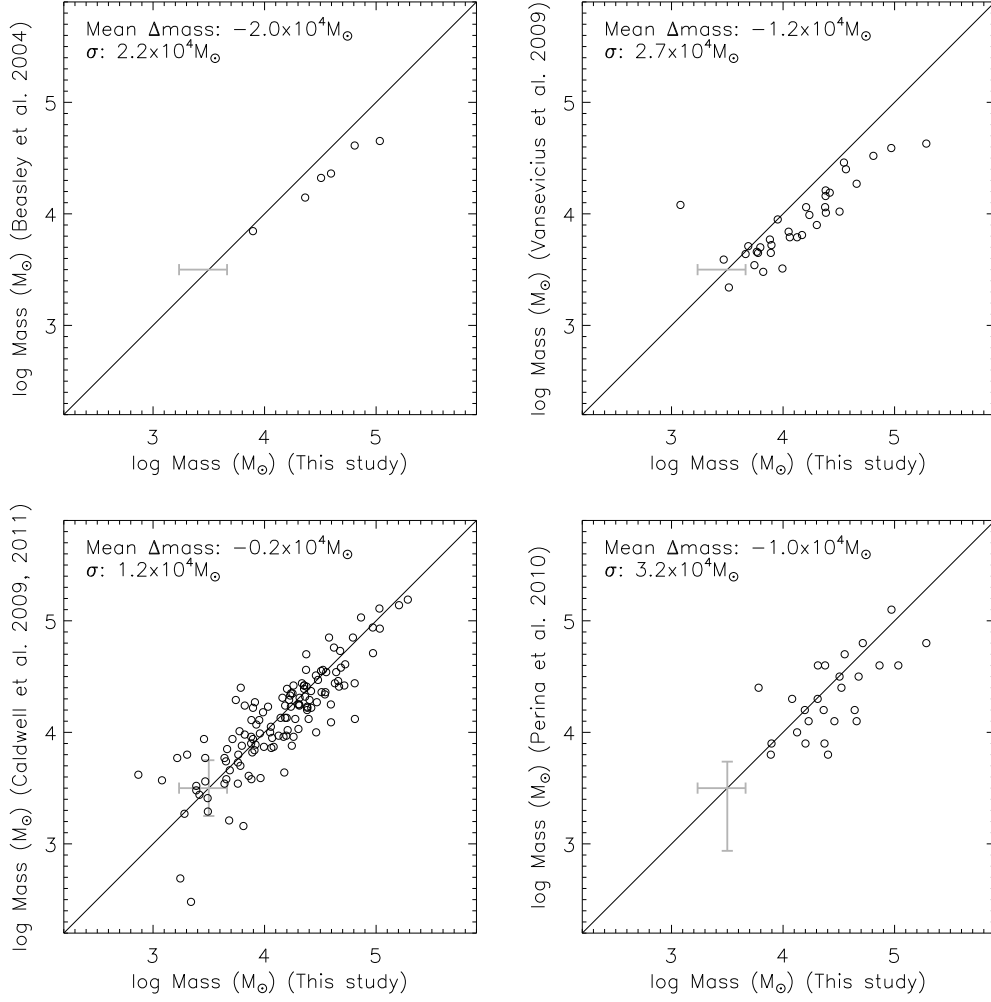


Fig. 9.— Comparison between cluster masses derived in this study and others: Beasley et al. (2004), Vansevicius et al. (2009), Caldwell et al. (2009, 2011), and Perina et al. (2010). In each plot, the mean value of mass difference (other study minus ours) is given with the standard deviation (σ). Error bars show median errors of cluster masses.

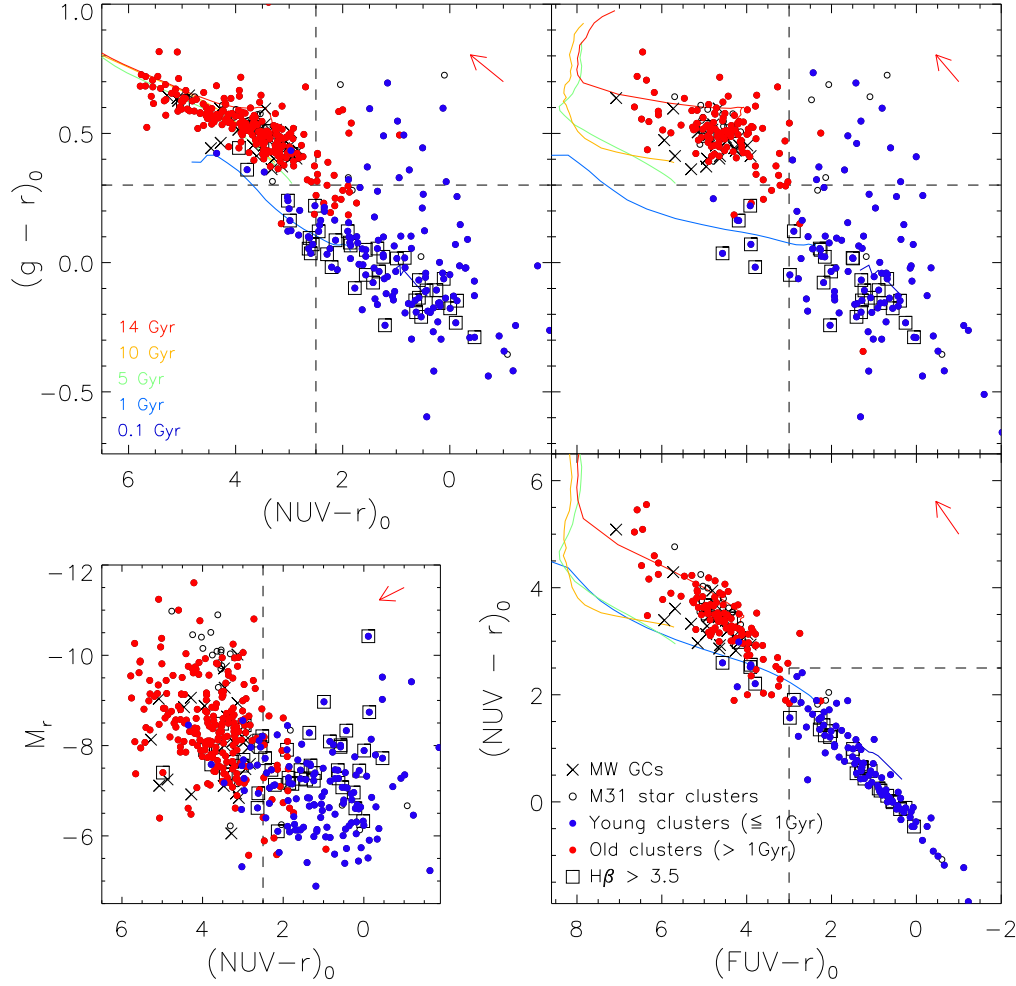


Fig. 10.— UV and optical color-color and color-magnitude diagrams of M31 star clusters. Blue and red filled circles are young (≤ 1 Gyr) and old (> 1 Gyr) clusters, respectively. Open circles are objects with no age estimates from our analysis. Open squares are clusters with $H\beta$ spectral index larger than 3.5 \AA . MW GCs are plotted with crosses. Solid curves are Yonsei evolutionary population models in the age range 0.1 - 14 Gyr. Horizontal and vertical dashed lines indicate reference values for dividing young and old clusters; $(FUV-r)_0 = 3.0$, $(NUV-r)_0 = 2.5$, and $(g-r)_0 = 0.3$. The arrow indicates a reddening vector for $E(B-V) = 0.10$ mag.

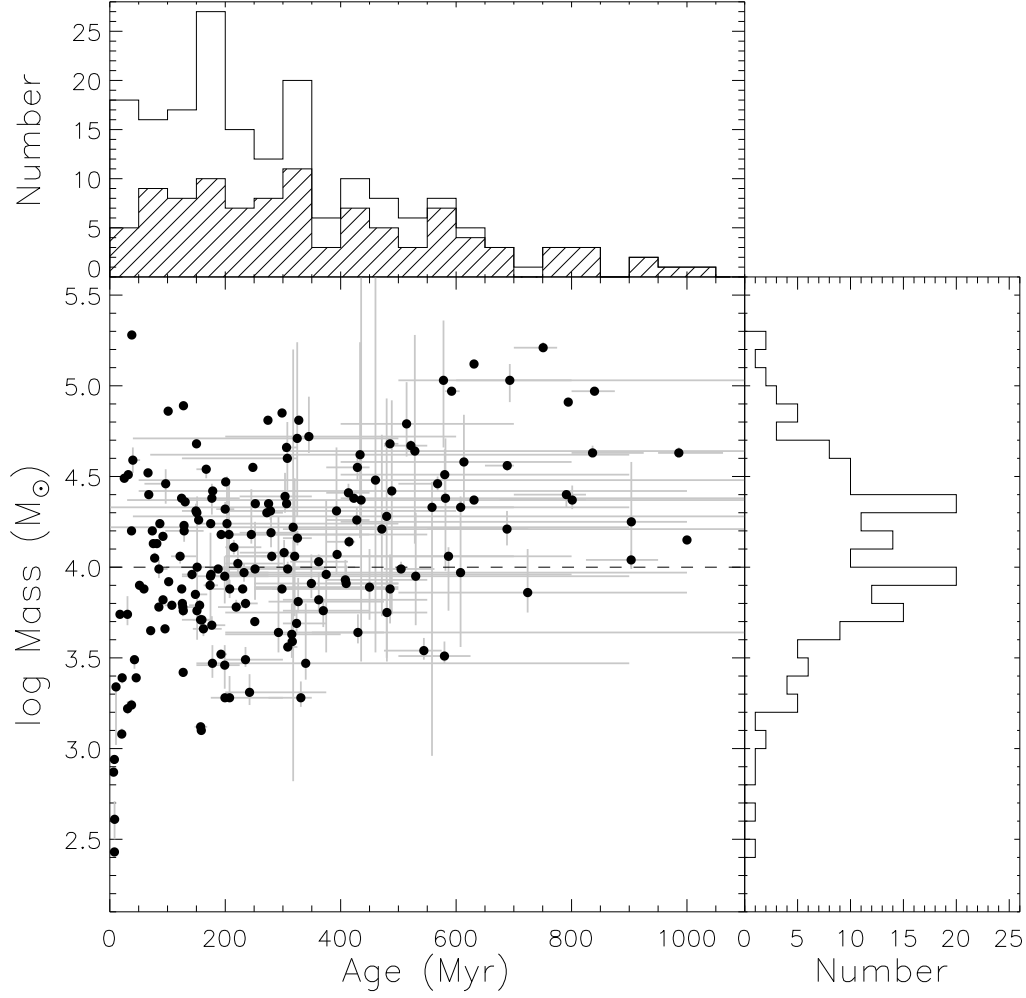


Fig. 11.— Age and mass distribution of 182 young clusters in M31. The hatched histogram is for clusters more massive than $10^4 M_{\odot}$. Error bars are uncertainties in the estimated ages and masses from χ^2 contours which are equal to minimum $(\chi^2) + 1$.

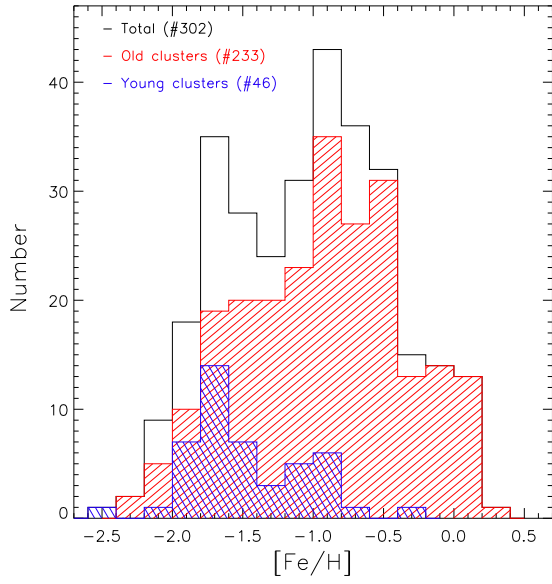


Fig. 12.— The metallicity distribution of the star clusters. Red and blue hatched histograms are for clusters older and younger than 1 Gyr, respectively. The black histogram is the distribution of the total cluster sample.

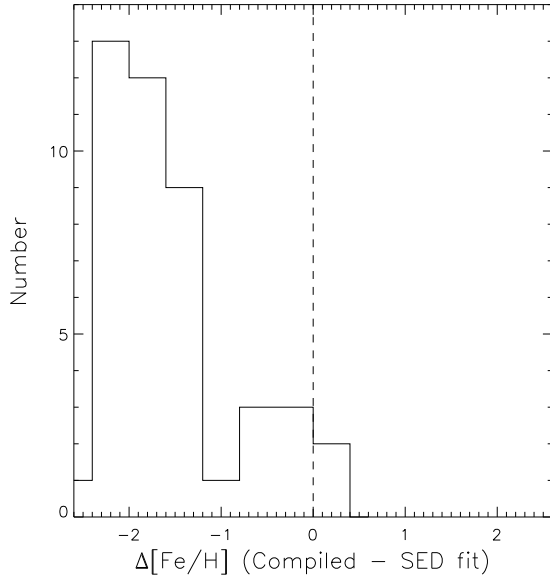


Fig. 13.— Metallicity differences of young clusters between our compiled values and values from our SED fitting.

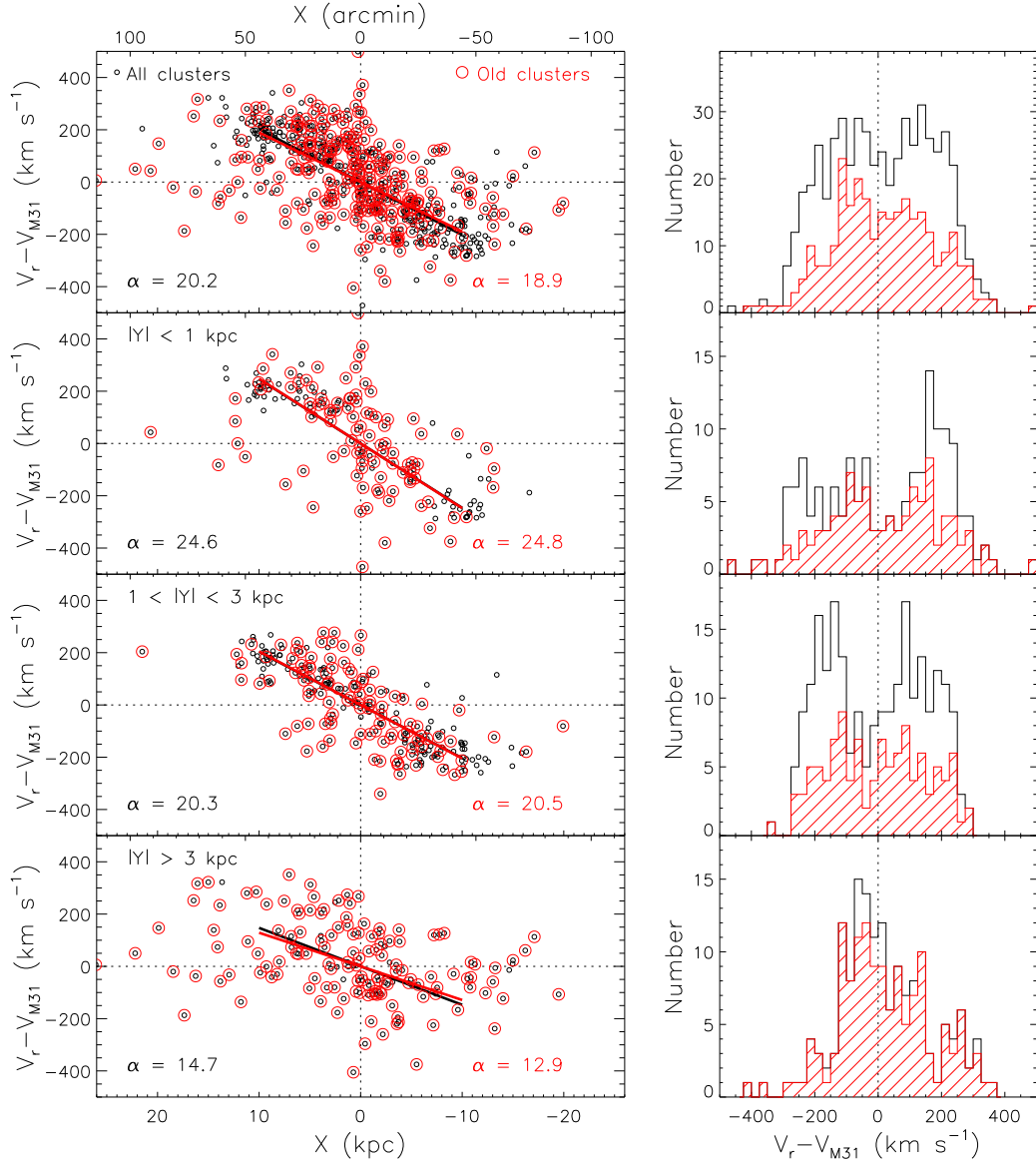


Fig. 14.— Radial velocities of 617 star clusters with respect to the M31 system velocity against the projected distance along the major axis (*black circles in left panels*) and their velocity distribution (*black histograms in right panels*). Red circles and hatched histograms are for old (> 1 Gyr) clusters. Solid lines in left panels are the linear fits to the sample within $|X| = 10$ kpc and α is the slope of the fit. Top panels show the star clusters over the whole region. Other panels are for the star clusters at different $|Y|$ ranges.

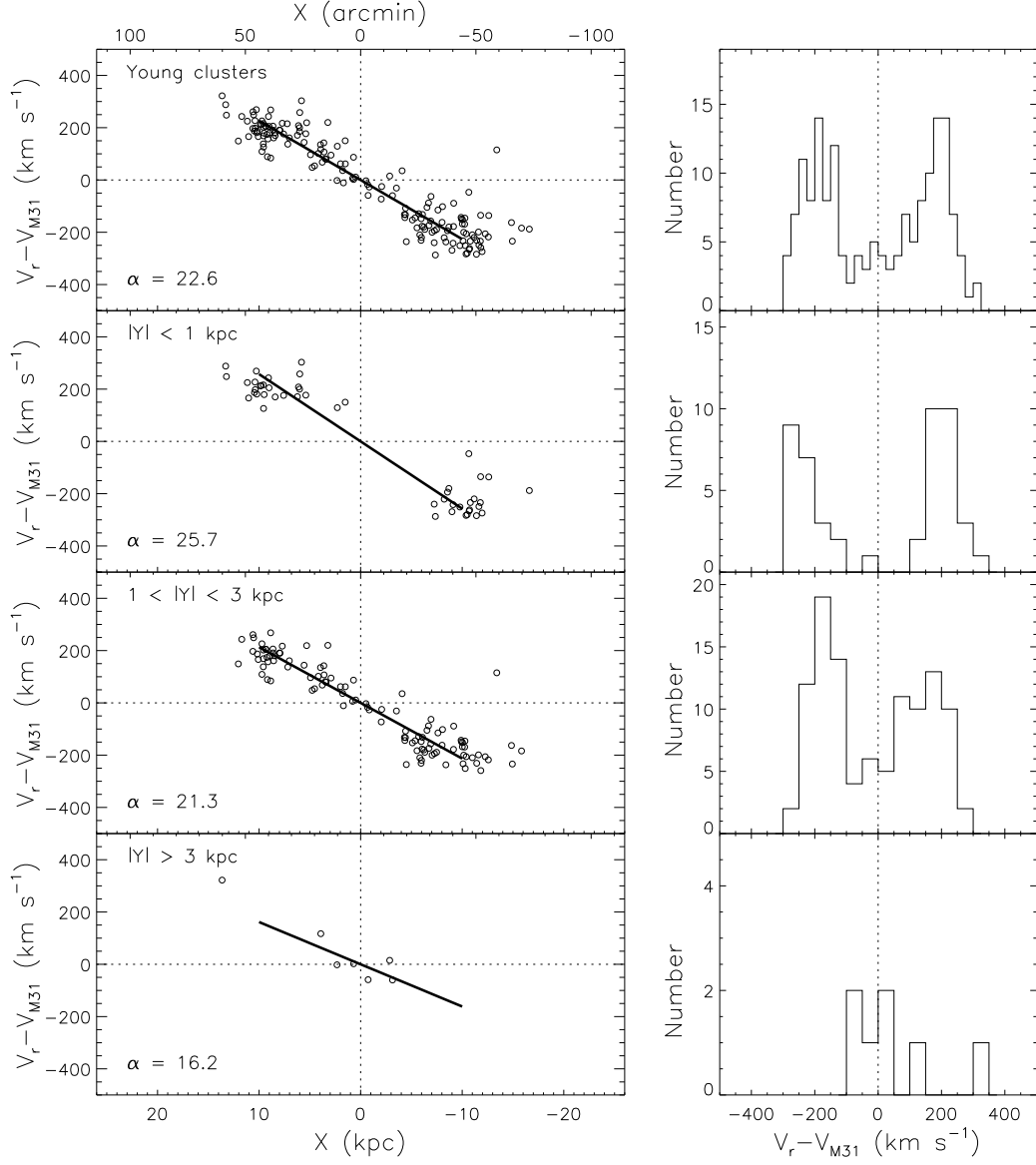


Fig. 15.— Same as Figure 14, but for young (≤ 1 Gyr) clusters.

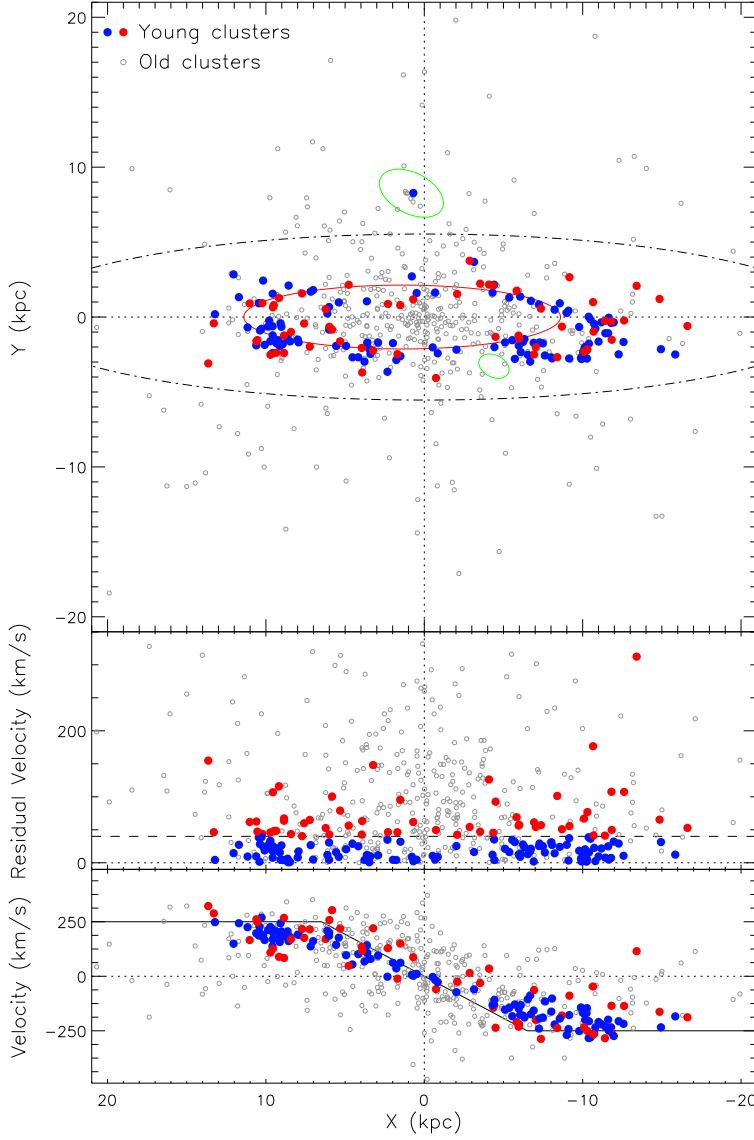


Fig. 16.— Spatial distribution (*top panel*) and kinematical properties (*middle and bottom panels*) of star clusters with available radial velocity. Colored filled circles are young clusters and small open circles are old clusters. (*middle panel*) We present residual velocities defined as absolute values of the difference between calculated velocities from cold-disk model and observed velocities. Two subgroups are separated by residual velocity of 40 km s^{-1} (dashed horizontal line). (*bottom panel*) Observed velocities corrected for the M31 system velocity against the projected distance along the major axis. The solid line is an adopted rotation curve that is flat with $V_{\text{circular}} = 250 \text{ km s}^{-1}$ for $|R| > 6.5 \text{ kpc}$ and then falls linearly to zero at $X = 0$.

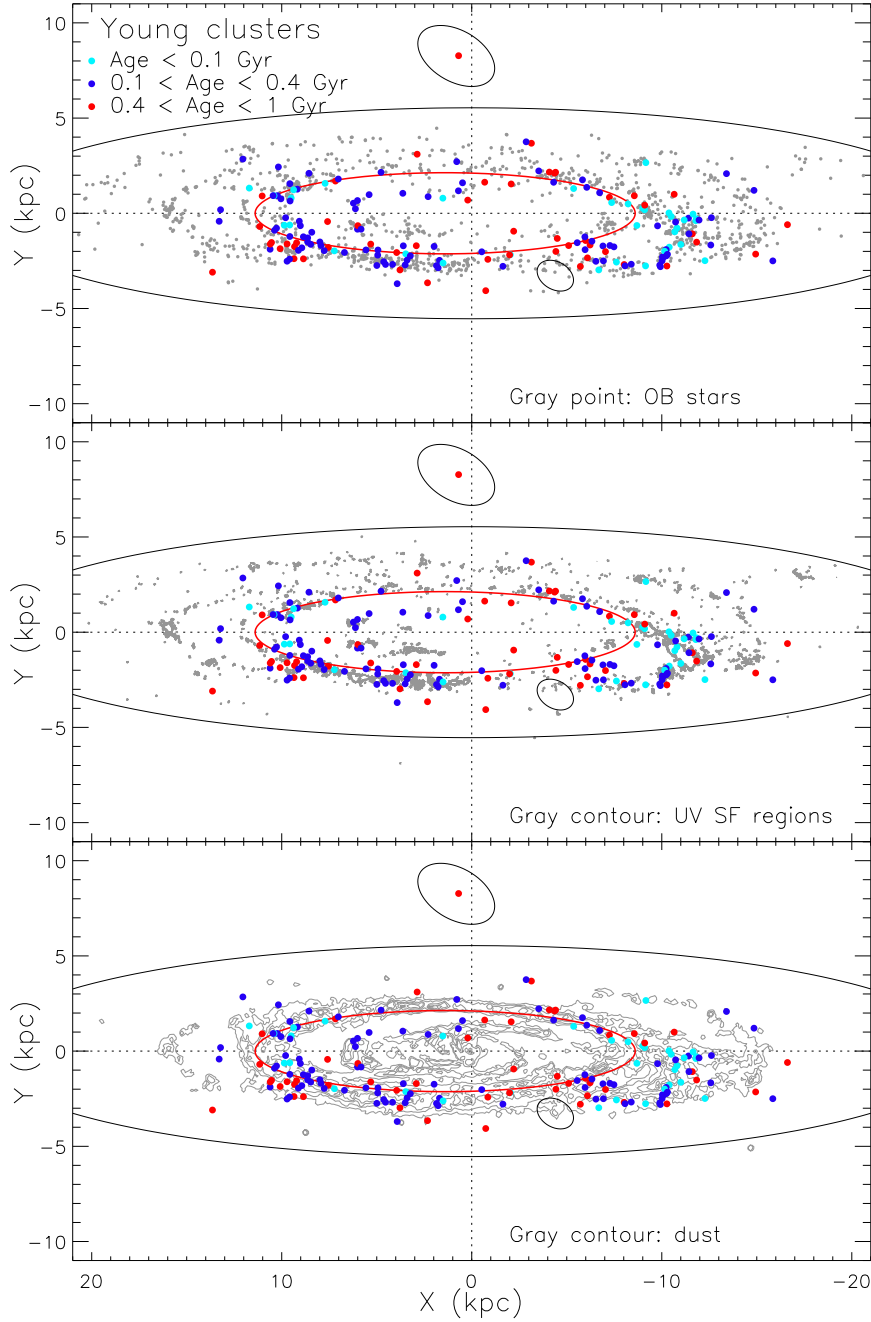


Fig. 17.— Spatial distribution of young clusters compared with OB stars (*top panel*), *GALEX* UV SF regions (*middle panel*), and *Spitzer* IRAC 8.0 μm IR contours (*bottom panel*, courtesy P. Barmby). Filled circles with different colors are young clusters in different age ranges; age < 100 Myr (cyan), 100 Myr < age < 400 Myr (blue), and 400 Myr < age < 1 Gyr (red).

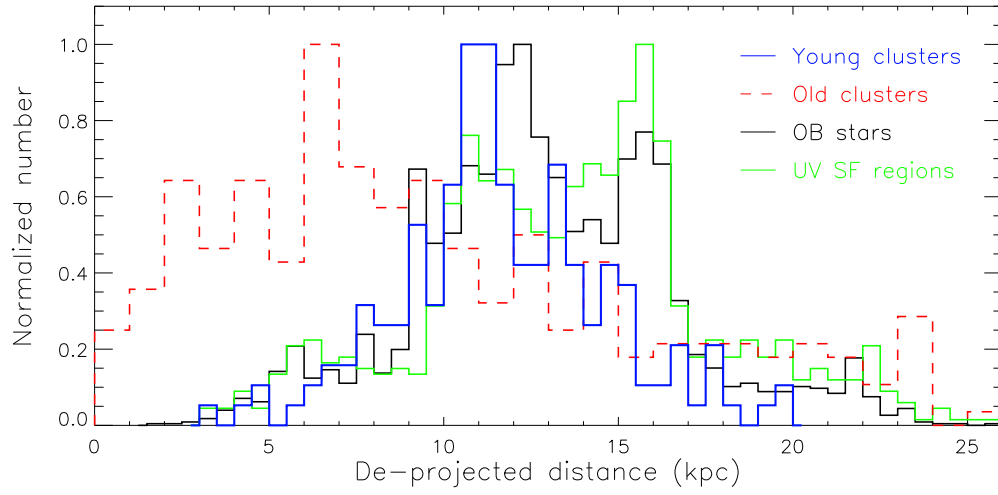


Fig. 18.— Number histogram of young clusters, old clusters, OB stars, and UV SF regions against de-projected distance from the center of M31.

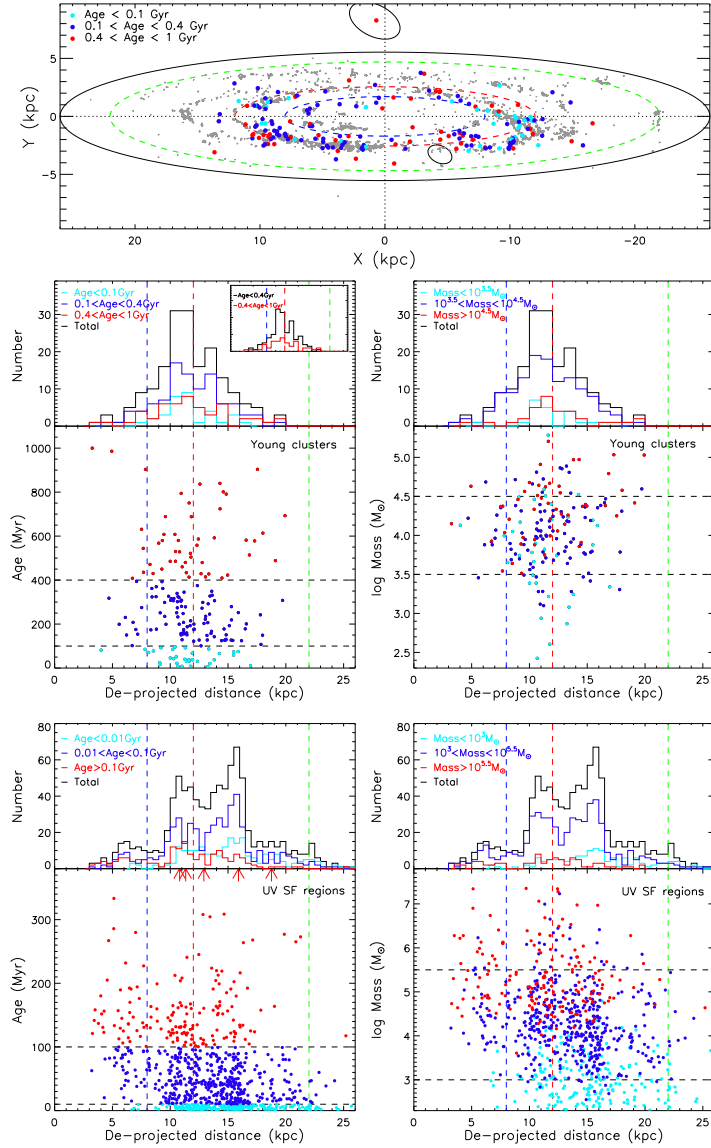


Fig. 19.— (*Top panel*) The spatial distribution of young clusters (red filled circles) and *GALEX* UV SF regions (yellow contours). (*Middle panels*) Distribution of ages (*left*) and masses (*right*) of young clusters against de-projected distance from the center of M31. In the inset of the left panel, two subsamples with different age range (age < 0.4 Gyr and 0.4 Gyr < age < 1 Gyr) are presented. (*Bottom panels*) Distribution of ages (*left*) and masses (*right*) of UV SF regions against de-projected distance from the center of M31. The dashed vertical lines correspond to the ellipses drawn on the top panel at 8, 12, and 22 kpc, respectively. Dots with different colors indicate star clusters in different age ranges (red: > 400 Myr, blue: 100 - 400 Myr, cyan: < 100 Myr) and SF regions (red: > 100 Myr, blue: 10 - 100 Myr, cyan: < 10 Myr).

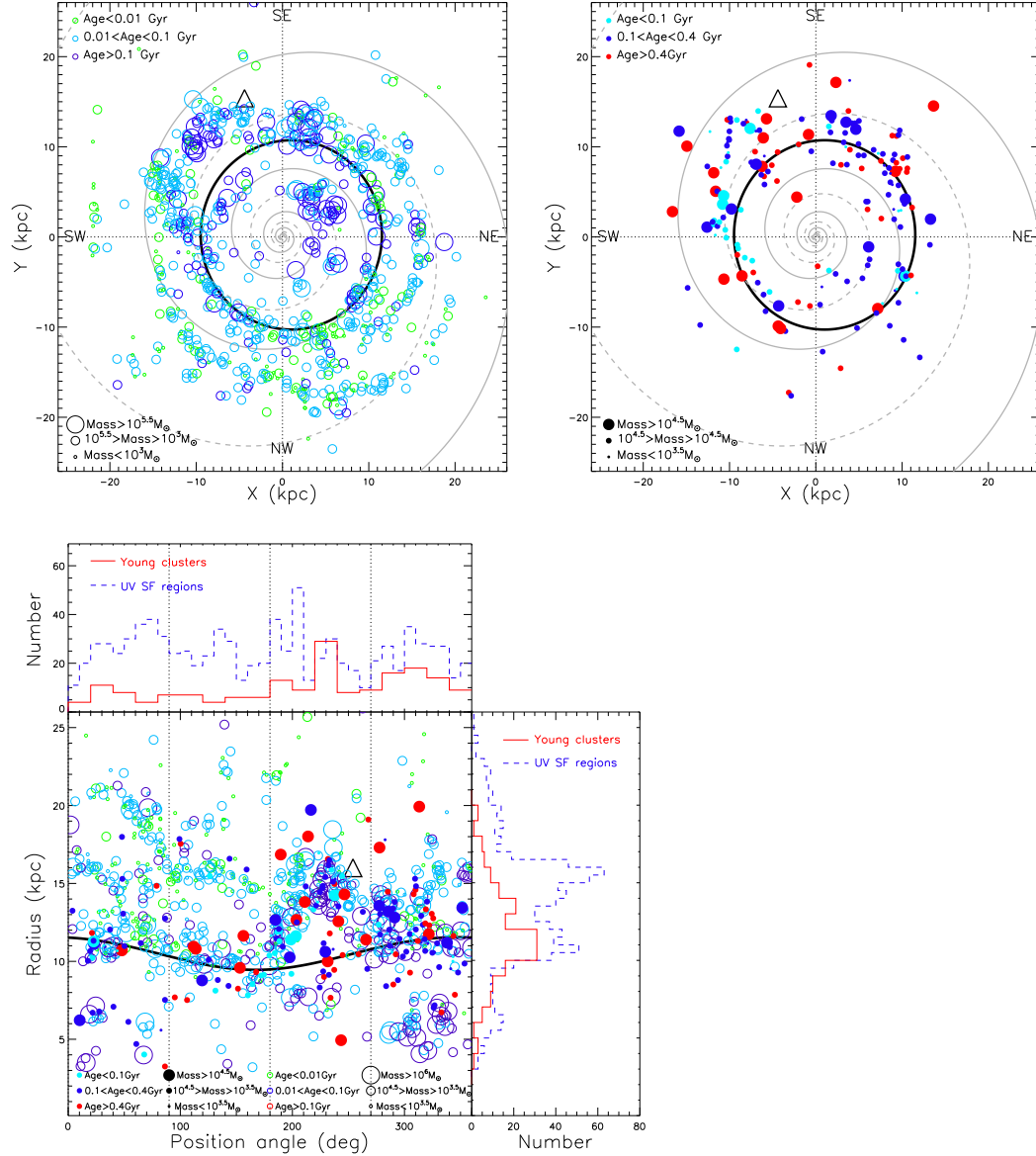


Fig. 20.— (*Upper panels*) De-projected spatial distribution of UV SF regions (left) and young clusters (right). Different colors and sizes indicate objects in different age and mass ranges. The black large circle is the 10 kpc star formation ring and two gray spirals are simple logarithmic spiral arms adopted from Gordon et al. (2006). (*Lower panel*) Spatial distribution of young clusters (filled circles) and SF regions (open circles) in polar coordinates. The black solid curve is the 10 kpc circular star formation ring. The triangle in each panel marks the location of M32.

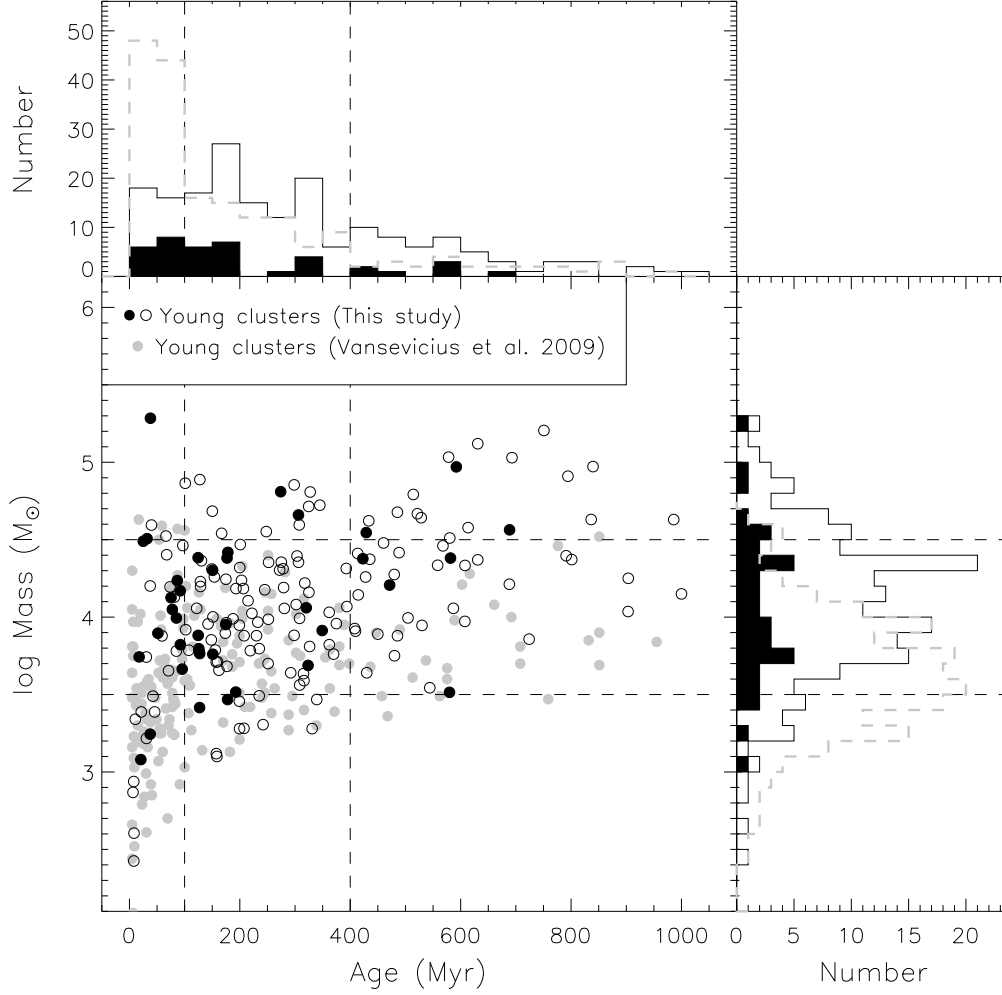


Fig. 21.— Age and mass distribution of our young cluster sample (black filled and open circles), and of compact star clusters (gray filled circles) from Vansevicius et al. (2009). Black filled circles are objects in common between our sample and that of Vansevicius et al. (2009). Age and mass histograms for different samples are also presented; all our young clusters (solid histogram), our young clusters in the field of Vansevicius et al. (2009) (filled histogram), and compact star clusters from Vansevicius et al. (2009) (gray dashed histogram).

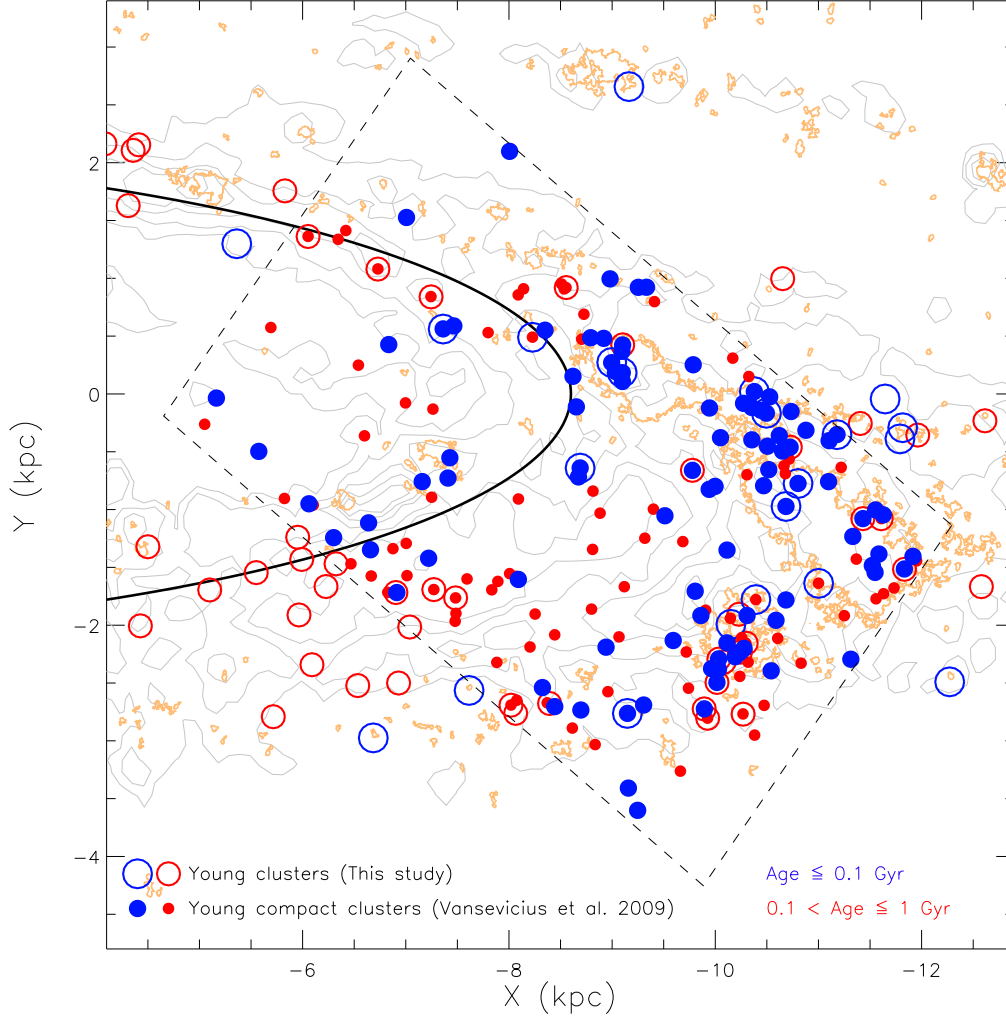


Fig. 22.— Spatial distribution of young clusters located in the southwestern part of the M31 disk. The large rectangle indicates the survey region of SUBARU Suprime-Cam by Vansevičius et al. (2009). Filled circles are young (≤ 1 Gyr) compact star clusters from Vansevičius et al. (2009) and open circles are our young clusters. Orange contours are UV SF regions from Kang et al. (2009) and gray contours are for the dust distribution from the *Spitzer* IRAC $8.0 \mu\text{m}$ image from Barmby et al. (2006). The large ellipse is the 10 kpc ring of the M31 disk.

Table 1. Merged catalog of star clusters in M31.

Name	RA	DEC	FUV	σ_{FUV}	NUV	σ_{NUV}	U	B	V	R	I	J	H	K_{RBC}	u	g	r	i	z	K_{P10}	$E(B-V)$	$\sigma_{E(B-V)}$	[Fe/H] ^a	$\sigma_{[Fe/H]}$	V_r	σ_{V_r}	f_{RBC}	f_{P10}	f_{C11}	f_{EBV}	
B001	00:39:51.01	40:58:10.6	18.82	18.33	17.06	16.47	15.41	14.68	13.73	13.86	19.38	17.58	16.61	16.07	15.69	13.72	0.25	0.02	-0.42	0.32	-191.1	14.3	1	1	3	1	
B002	00:40:02.58	41:11:53.5	21.28	0.04	18.14	18.18	17.55	17.12	16.58	14.87	14.77	...	19.15	17.86	17.34	17.06	16.90	15.47	0.01	0.04	99.99	99.99	-338.2	14.5	1	1	3	1	
B003	00:40:09.41	41:11:05.7	23.06	0.20	21.55	0.04	18.40	18.35	17.57	17.07	16.41	15.96	15.16	15.54	19.43	17.94	17.36	16.99	16.82	15.09	0.16	0.04	-0.99	0.48	-364.0	15.3	1	1	3	1	
B004	00:40:17.92	41:22:40.3	22.25	0.07	18.29	17.87	16.95	16.36	15.73	14.96	14.24	14.10	19.06	17.40	16.64	16.27	16.05	14.17	0.13	0.03	-1.00	0.41	-369.4	13.4	1	1	3	1	
B005	00:40:20.32	40:43:58.3	21.03	0.07	16.85	16.64	15.69	15.02	14.40	13.39	12.68	12.53	17.87	16.12	15.32	14.90	14.62	12.56	0.22	0.05	-0.82	0.38	-278.3	12.8	1	1	3	1	
B006	00:40:26.49	41:27:26.7	21.41	0.04	16.94	16.49	15.50	14.97	14.33	13.47	12.74	12.63	17.68	15.92	15.16	14.78	14.52	12.55	0.11	0.03	-0.59	0.41	-234.7	5.8	1	1	3	1	
B008	00:40:30.29	41:16:08.7	22.59	0.12	18.16	17.66	16.56	16.21	15.51	14.66	14.05	13.89	19.03	17.23	16.47	16.07	15.85	14.02	0.17	0.09	-0.47	0.35	-318.5	12.6	1	1	3	2	
B009	00:40:30.70	41:36:55.6	23.09	0.15	20.96	0.03	17.54	17.63	16.92	16.42	15.87	15.27	14.47	14.42	18.55	17.24	16.63	16.33	16.19	14.67	0.09	0.04	-1.55	0.23	-325.5	52.9	1	1	3	1	
B010	00:40:31.57	41:14:22.5	21.93	0.08	20.87	0.03	17.65	17.50	16.66	16.12	15.48	14.83	14.28	13.98	18.45	17.03	16.38	16.02	15.80	14.16	0.20	0.03	-1.64	0.68	-162.7	14.7	1	1	3	1	
B011	00:40:31.88	41:39:16.9	21.84	0.06	20.58	0.02	17.59	17.39	16.58	16.10	15.56	14.85	14.23	14.08	18.42	17.06	16.43	16.14	15.97	14.17	0.09	0.04	-1.71	0.24	-207.9	53.7	1	1	3	1	
B012	00:40:32.47	41:21:44.2	20.10	0.02	19.02	0.01	15.99	15.86	15.09	14.62	14.03	13.36	12.78	12.74	16.76	15.43	14.83	14.52	14.35	12.73	0.11	0.02	-1.91	0.21	-359.4	11.3	1	1	3	1	
B013	00:40:38.44	41:25:23.7	23.21	0.25	18.56	18.06	17.19	16.60	15.96	15.22	14.46	14.22	19.19	17.63	16.88	16.47	16.19	14.44	0.13	0.06	-0.74	0.51	-410.2	13.2	1	1	3	1	
B015	00:40:45.03	40:59:56.1	19.20	17.79	16.93	15.90	14.61	13.75	13.44	20.74	18.61	17.43	16.70	16.26	13.67	0.61	0.03	0.37	0.02	-460.0	14.0	1	1	3	1	
B016	00:40:45.17	41:22:09.9	23.46	0.24	18.86	18.58	17.58	16.85	16.15	15.15	14.17	14.08	19.98	17.99	17.18	16.74	16.42	14.44	0.35	0.04	-0.53	0.34	-397.2	13.2	1	1	3	1	
B017	00:40:48.72	41:12:07.2	21.57	0.13	17.55	17.04	15.95	15.23	14.51	13.47	12.69	12.60	18.27	16.48	15.51	14.97	14.59	12.53	0.32	0.03	-0.82	0.24	-522.2	9.8	1	1	3	1	
...

Note. — This table is available in its entirety in the electronic edition of the online journal. A portion is shown here for guidance regarding its format and content.

^aValues in parentheses are either from Beasley et al. (2004) or Perina et al. (2010), or the mean of these values (for B222, B321, and B327).

Table 2. Catalog of 182 young clusters.

Name	RA	DEC	Age	Log Mass	$E(B - V)$	f_{EBV}^a	Z^b	Flag ^c
	(hh:mm:ss)	(dd:mm:ss)	(Myr)	(M_{\odot})	(mag)			
B040	0:41:38.86	40:40:54.4	422	4.38	0.00	2	0.004	1
B043	0:41:42.31	40:42:39.8	66	4.52	0.24	1	0.05	1
B049	0:41:45.58	40:49:55.0	485	4.68	0.21	1	0.02	1
B066	0:42:03.09	40:44:47.1	73	4.20	0.14	1	0.05	1
B069	0:42:05.52	41:26:09.2	272	4.30	0.19	1	0.05	1
B081	0:42:13.59	40:48:39.0	839	4.97	0.17	2	0.004	1
B091	0:42:21.71	41:22:05.3	275	4.35	0.11	2	0.05	1
B133	0:42:51.60	41:23:29.7	81	4.13	0.01	2	0.05	2
B192	0:43:44.52	41:37:27.0	393	4.07	0.00	2	0.02	1
B195	0:43:48.55	41:02:27.9	488	4.42	0.36	2	0.0004	1
...

Note. — This table is available in its entirety in the electronic edition of the online journal. A portion is shown here for guidance regarding its format and content.

^aFlag of $E(B - V)$: (1) reddening value from our compiled catalog (*indivEBV*), (2) reddening value from our SED fitting (*freeEBV*).

^bMetallicity adopted in SED fitting (see Section 3.1).

^cYoung clusters flag: (1) young clusters in both this work and Caldwell et al. (2009), (2)

only in this work, (3) only in Caldwell et al. (2009).